The Impact of Climate Forcing Biases and the Nitrogen Cycle on Land Carbon Balance Projections

Christian Seiler[1], Sian Kou-Giesbrecht[2], Vivek Arora[2], and Joe R. Melton[3]

[1]Queen's University
[2]Canadian Centre for Climate Modelling and Analysis
[3]Environment Canada

April 16, 2023

Abstract

Earth System Models (ESMs) project that the terrestrial carbon sink will continue to grow as atmospheric CO_2 increases, but this projection is uncertain due to biases in the simulated climate and how ESMs represent ecosystem processes. In particular, the strength of the CO_2 fertilization effect, which is modulated by nutrient cycles, varies substantially across models. This study evaluates land carbon balance uncertainties for the Canadian Earth System Model (CanESM) by conducting simulations where the latest version of CanESM's land surface component is driven offline with raw and bias-adjusted CanESM5 climate forcing data. To quantify the impact of nutrient limitation, we complete simulations where the nitrogen cycle is enabled or disabled. Results show that bias adjustment improves model performance across most ecosystem variables, primarily due to reduced biases in precipitation. Turning the nitrogen cycle on increases the global land carbon sink during the historical period (1995-2014) due to enhanced nitrogen deposition, placing it within the Global Carbon Budget uncertainty range. During the future period (2080-2099), the simulated land carbon sink increases in response to bias adjustment and decreases in response to the dynamic carbon-nitrogen interaction, leading to a net decrease when both factors are acting together. The dominating impact of the nitrogen cycle demonstrates the importance of representing nutrient limitation in ESMs. Such efforts may produce more robust carbon balance projections in support of global climate change mitigation policies such as the 2015 Paris Agreement.

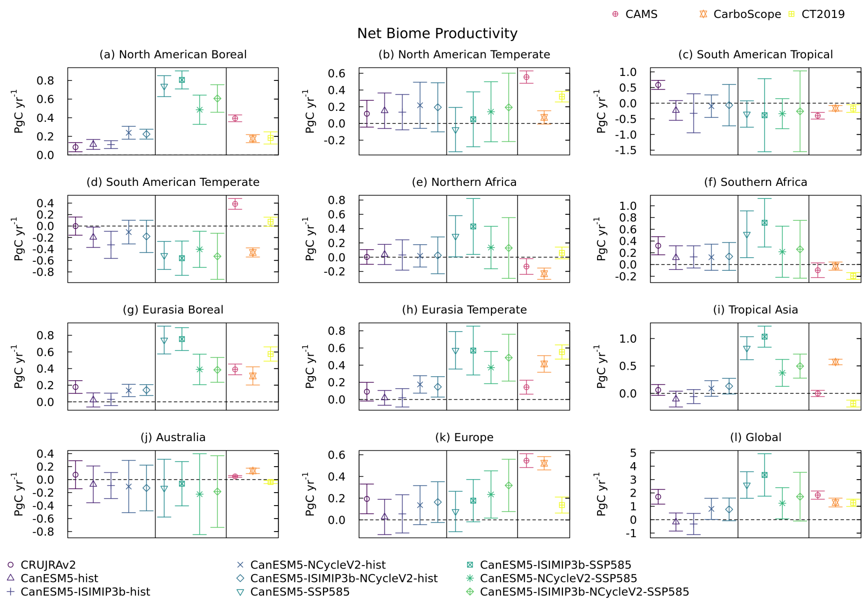

CAMS
CarboScope
CT2019
Net Biome Productivity
(a) North American Boreal
(b) North American Temperate
(c) South American Tropical
(d) South American Temperate
(e) Northern Africa
(f) Southern Africa
(g) Eurasia Boreal
(h) Eurasia Temperate
(i) Tropical Asia
(j) Australia
(k) Europe
(l) Global
PgC yr-1
CRUJRAv2
CanESM5-hist
CanESM5-ISIMIP3b-hist
CanESM5-NCycleV2-hist
CanESM5-ISIMIP3b-NCycleV2-hist
CanESM5-SSP585
CanESM5-ISIMIP3b-SSP585
CanESM5-NCycleV2-SSP585
CanESM5-ISIMIP3b-NCycleV2-SSP585

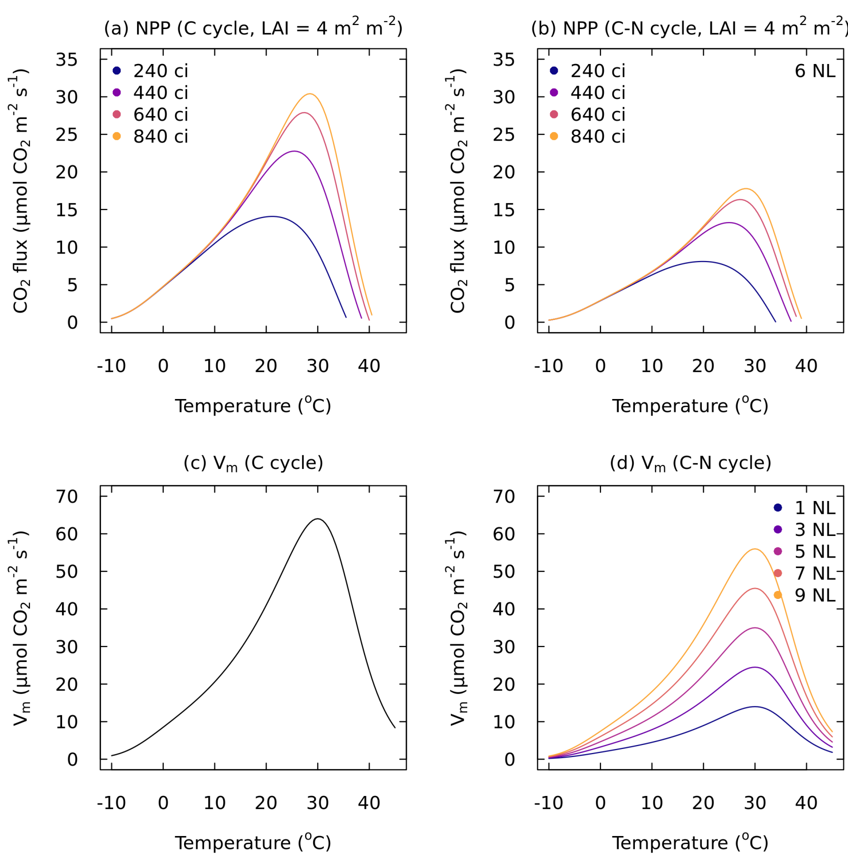

(a) NPP (C cycle, LAI = 4 m2 m-2)
(b) NPP (C-N cycle, LAI = 4 m2 m-2)
240 ci
440 ci
640 ci
840 ci
6 NL
CO2 flux (µmol CO2 m-2 s-1)
Temperature (oC)
(c) Vm (C cycle)
(d) Vm (C-N cycle)
1 NL
3 NL
5 NL
7 NL
9 NL
Vm (µmol CO2 m-2 s-1)
Temperature (oC)

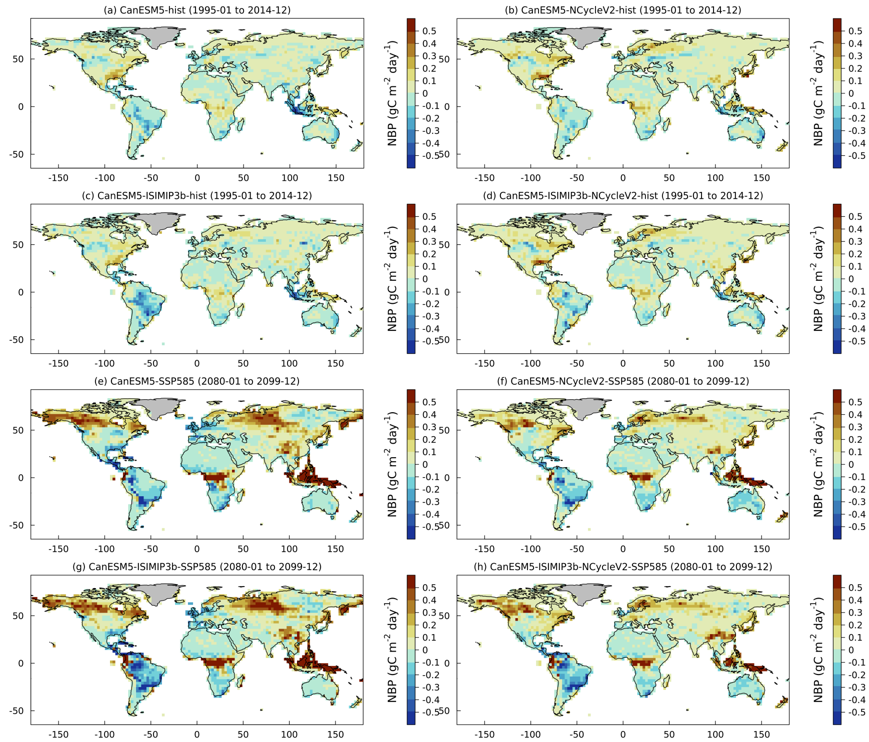
(a) CanESM5-hist (1995-01 to 2014-12)
(b) CanESM5-NCycleV2-hist (1995-01 to 2014-12)
(c) CanESM5-ISIMIP3b-hist (1995-01 to 2014-12)
(d) CanESM5-ISIMIP3b-NCycleV2-hist (1995-01 to 2014-12)
(e) CanESM5-SSP585 (2080-01 to 2099-12)
(f) CanESM5-NCycleV2-SSP585 (2080-01 to 2099-12)
(g) CanESM5-ISIMIP3b-SSP585 (2080-01 to 2099-12)
(h) CanESM5-ISIMIP3b-NCycleV2-SSP585 (2080-01 to 2099-12)
NBP (gC m^{-2} day^{-1})

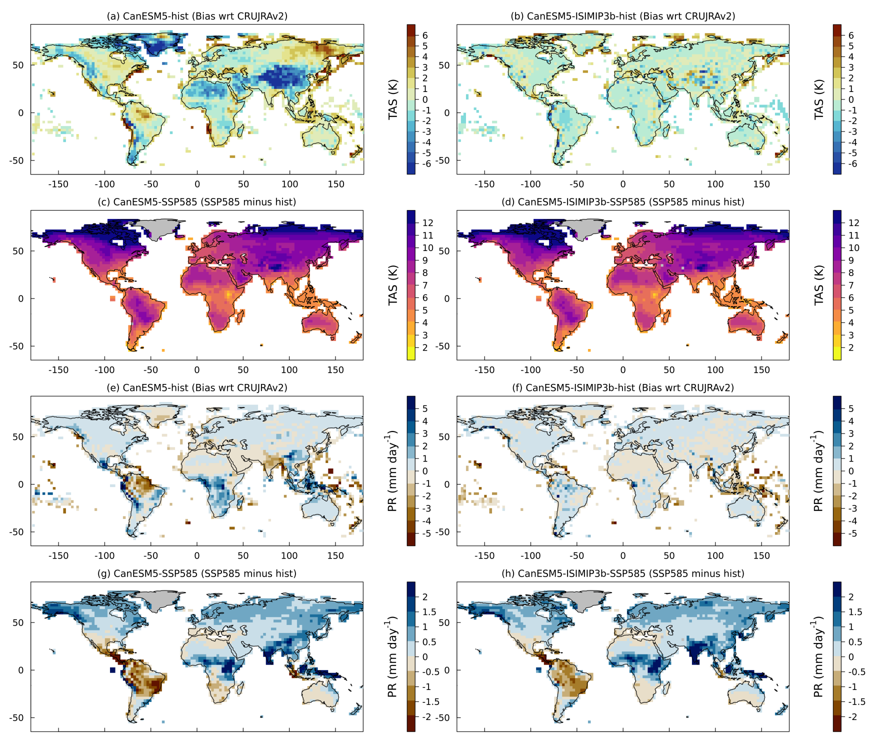
(a) CanESM5-hist (Bias wrt CRUJRAv2)
(b) CanESM5-ISIMIP3b-hist (Bias wrt CRUJRAv2)
TAS (K)
(c) CanESM5-SSP585 (SSP585 minus hist)
(d) CanESM5-ISIMIP3b-SSP585 (SSP585 minus hist)
TAS (K)
(e) CanESM5-hist (Bias wrt CRUJRAv2)
(f) CanESM5-ISIMIP3b-hist (Bias wrt CRUJRAv2)
PR (mm day^{-1})
(g) CanESM5-SSP585 (SSP585 minus hist)
(h) CanESM5-ISIMIP3b-SSP585 (SSP585 minus hist)
PR (mm day^{-1})

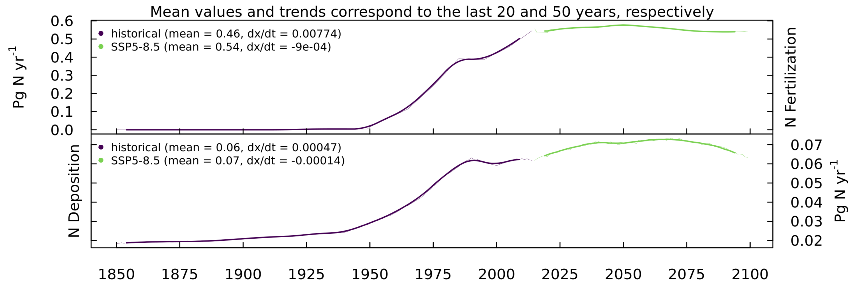
Mean values and trends correspond to the last 20 and 50 years, respectively
historical (mean = 0.46, dx/dt = 0.00774)
SSP5-8.5 (mean = 0.54, dx/dt = -9e-04)
historical (mean = 0.06, dx/dt = 0.00047)
SSP5-8.5 (mean = 0.07, dx/dt = -0.00014)
N Fertilization
N Deposition
Pg N yr-1

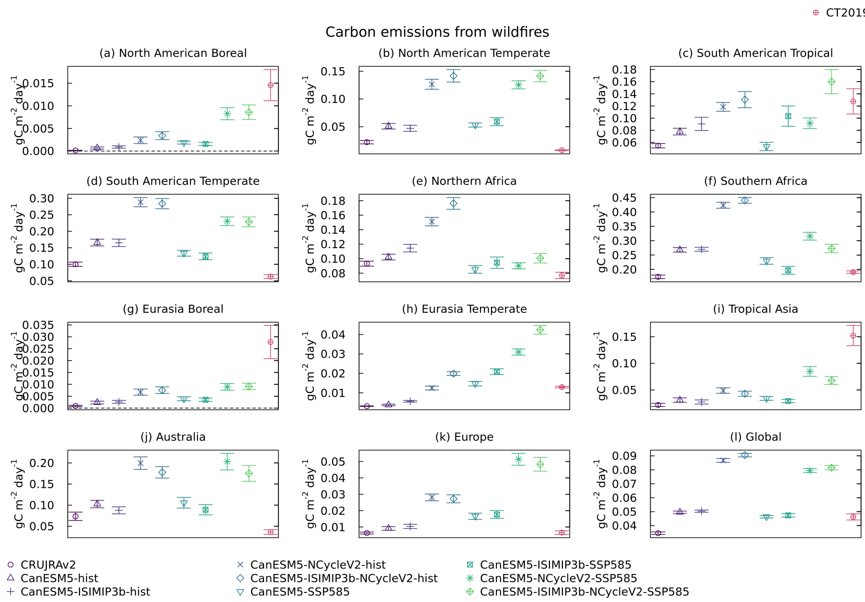
Carbon emissions from wildfires
CT2019
(a) North American Boreal
(b) North American Temperate
(c) South American Tropical
(d) South American Temperate
(e) Northern Africa
(f) Southern Africa
(g) Eurasia Boreal
(h) Eurasia Temperate
(i) Tropical Asia
(j) Australia
(k) Europe
(l) Global
gC m-2 day-1
CRUJRAv2
CanESM5-hist
CanESM5-ISIMIP3b-hist
CanESM5-NCycleV2-hist
CanESM5-ISIMIP3b-NCycleV2-hist
CanESM5-SSP585
CanESM5-ISIMIP3b-SSP585
CanESM5-NCycleV2-SSP585
CanESM5-ISIMIP3b-NCycleV2-SSP585

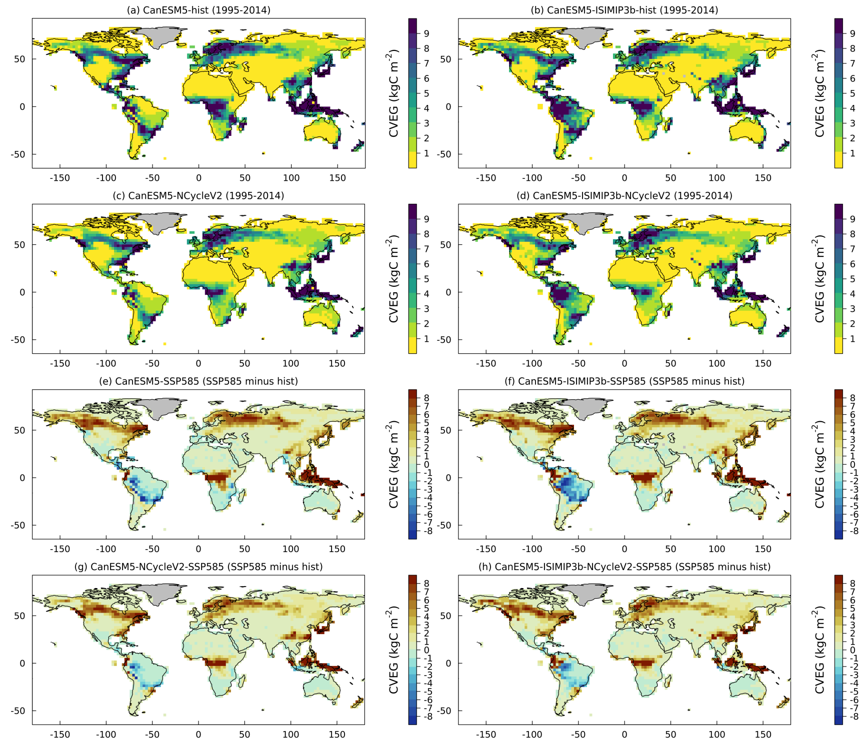
(a) CanESM5-hist (1995-2014)
(b) CanESM5-ISIMIP3b-hist (1995-2014)
(c) CanESM5-NCycleV2 (1995-2014)
(d) CanESM5-ISIMIP3b-NCycleV2 (1995-2014)
(e) CanESM5-SSP585 (SSP585 minus hist)
(f) CanESM5-ISIMIP3b-SSP585 (SSP585 minus hist)
(g) CanESM5-NCycleV2-SSP585 (SSP585 minus hist)
(h) CanESM5-ISIMIP3b-NCycleV2-SSP585 (SSP585 minus hist)
CVEG (kgC m^{-2})

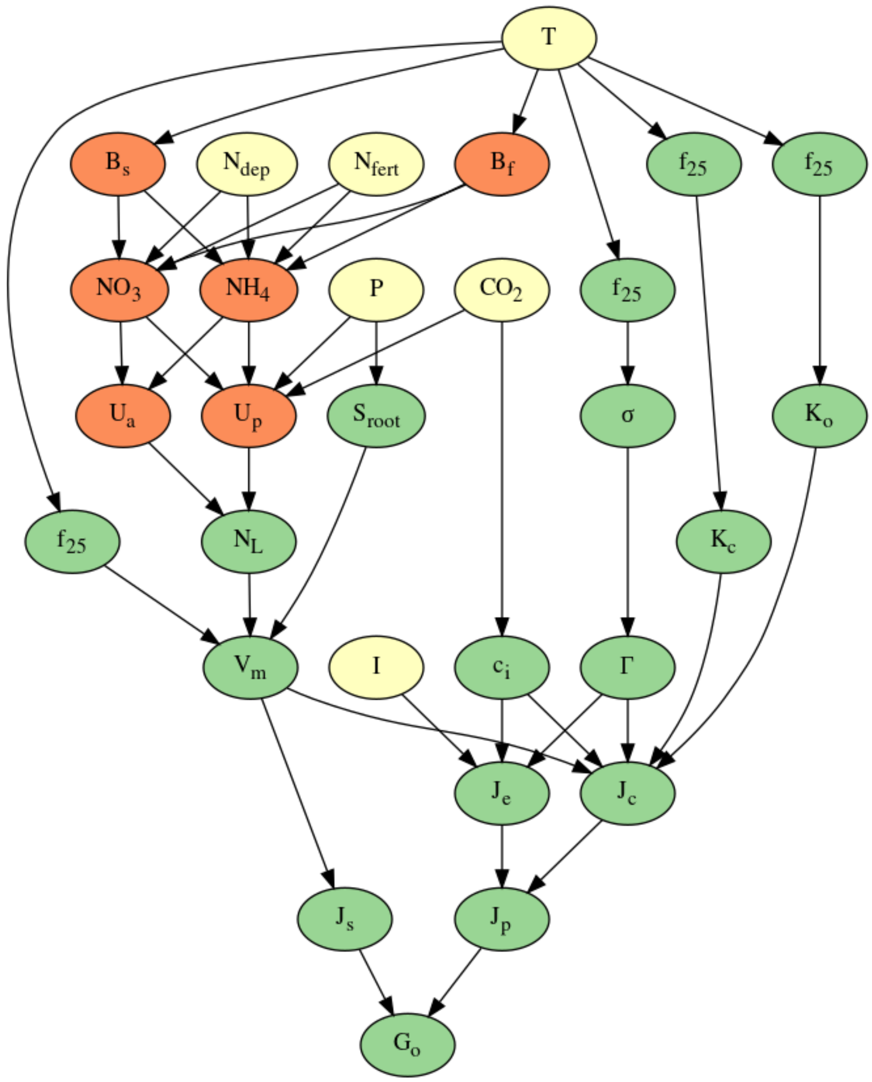
T
B_s
N_dep
N_fert
B_f
f_25
f_25
NO_3
NH_4
P
CO_2
f_25
U_a
U_p
S_root
σ
K_o
f_25
N_L
K_c
V_m
I
c_i
Γ
J_e
J_c
J_s
J_p
G_o

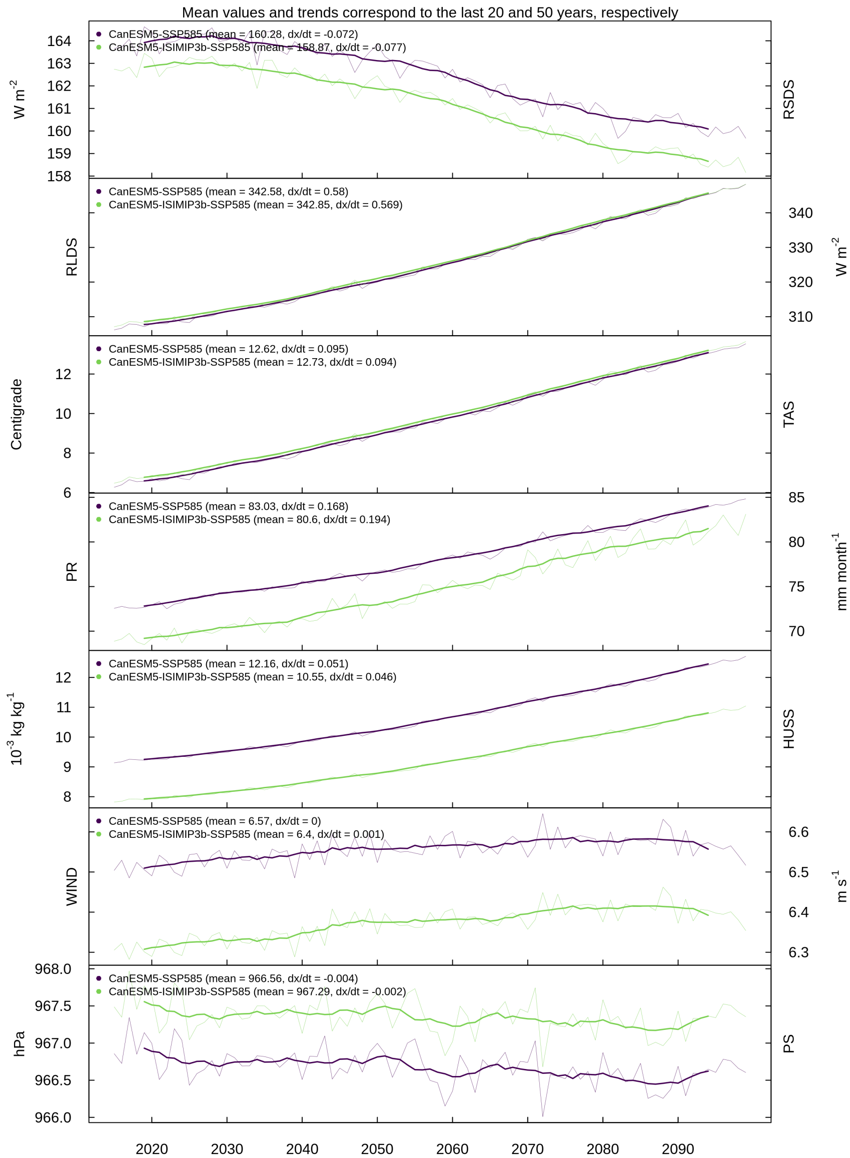
Mean values and trends correspond to the last 20 and 50 years, respectively
CanESM5-SSP585 (mean = 160.28, dx/dt = -0.072)
CanESM5-ISIMIP3b-SSP585 (mean = 158.87, dx/dt = -0.077)
RSDS
CanESM5-SSP585 (mean = 342.58, dx/dt = 0.58)
CanESM5-ISIMIP3b-SSP585 (mean = 342.85, dx/dt = 0.569)
RLDS
CanESM5-SSP585 (mean = 12.62, dx/dt = 0.095)
CanESM5-ISIMIP3b-SSP585 (mean = 12.73, dx/dt = 0.094)
TAS
Centigrade
CanESM5-SSP585 (mean = 83.03, dx/dt = 0.168)
CanESM5-ISIMIP3b-SSP585 (mean = 80.6, dx/dt = 0.194)
PR
mm month-1
CanESM5-SSP585 (mean = 12.16, dx/dt = 0.051)
CanESM5-ISIMIP3b-SSP585 (mean = 10.55, dx/dt = 0.046)
HUSS
10-3 kg kg-1
CanESM5-SSP585 (mean = 6.57, dx/dt = 0)
CanESM5-ISIMIP3b-SSP585 (mean = 6.4, dx/dt = 0.001)
WIND
m s-1
CanESM5-SSP585 (mean = 966.56, dx/dt = -0.004)
CanESM5-ISIMIP3b-SSP585 (mean = 967.29, dx/dt = -0.002)
PS
hPa
W m-2
2020
2030
2040
2050
2060
2070
2080
2090

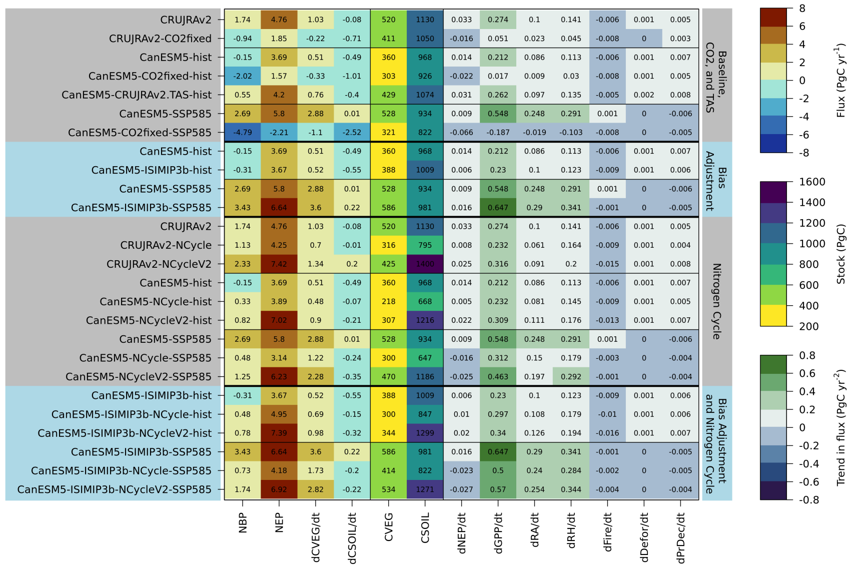

	NBP	NEP	dCVEG/dt	dCSOIL/dt	CVEG	CSOIL	dNEP/dt	dGPP/dt	dRA/dt	dRH/dt	dFire/dt	dDefor/dt	dPrDec/dt	
CRUJRAv2	1.74	4.76	1.03	-0.08	520	1130	0.033	0.274	0.1	0.141	-0.006	0.001	0.005	Baseline, CO2, and TAS
CRUJRAv2-CO2fixed	-0.94	1.85	-0.22	-0.71	411	1050	-0.016	0.051	0.023	0.045	-0.008	0	0.003	
CanESM5-hist	-0.15	3.69	0.51	-0.49	360	968	0.014	0.212	0.086	0.113	-0.006	0.001	0.007	
CanESM5-CO2fixed-hist	-2.02	1.57	-0.33	-1.01	303	926	-0.022	0.017	0.009	0.03	-0.008	0.001	0.005	
CanESM5-CRUJRAv2.TAS-hist	0.55	4.2	0.76	-0.4	429	1074	0.031	0.262	0.097	0.135	-0.005	0.002	0.008	
CanESM5-SSP585	2.69	5.8	2.88	0.01	528	934	0.009	0.548	0.248	0.291	0.001	0	-0.006	
CanESM5-CO2fixed-SSP585	-4.79	-2.21	-1.1	-2.52	321	822	-0.066	-0.187	-0.019	-0.103	-0.008	0	-0.005	
CanESM5-hist	-0.15	3.69	0.51	-0.49	360	968	0.014	0.212	0.086	0.113	-0.006	0.001	0.007	Bias Adjustment
CanESM5-ISIMIP3b-hist	-0.31	3.67	0.52	-0.55	388	1009	0.006	0.23	0.1	0.123	-0.009	0.001	0.006	
CanESM5-SSP585	2.69	5.8	2.88	0.01	528	934	0.009	0.548	0.248	0.291	0.001	0	-0.006	
CanESM5-ISIMIP3b-SSP585	3.43	6.64	3.6	0.22	586	981	0.016	0.647	0.29	0.341	-0.001	0	-0.005	
CRUJRAv2	1.74	4.76	1.03	-0.08	520	1130	0.033	0.274	0.1	0.141	-0.006	0.001	0.005	Nitrogen Cycle
CRUJRAv2-NCycle	1.13	4.25	0.7	-0.01	316	795	0.008	0.232	0.061	0.164	-0.009	0.001	0.004	
CRUJRAv2-NCycleV2	2.33	7.42	1.34	0.2	425	1400	0.025	0.316	0.091	0.2	-0.015	0.001	0.008	
CanESM5-hist	-0.15	3.69	0.51	-0.49	360	968	0.014	0.212	0.086	0.113	-0.006	0.001	0.007	
CanESM5-NCycle-hist	0.33	3.89	0.48	-0.07	218	668	0.005	0.232	0.081	0.145	-0.009	0.001	0.005	
CanESM5-NCycleV2-hist	0.82	7.02	0.9	-0.21	307	1216	0.022	0.309	0.111	0.176	-0.013	0.001	0.007	
CanESM5-SSP585	2.69	5.8	2.88	0.01	528	934	0.009	0.548	0.248	0.291	0.001	0	-0.006	
CanESM5-NCycle-SSP585	0.48	3.14	1.22	-0.24	300	647	-0.016	0.312	0.15	0.179	-0.003	0	-0.004	
CanESM5-NCycleV2-SSP585	1.25	6.23	2.28	-0.35	470	1186	-0.025	0.463	0.197	0.292	-0.001	0	-0.004	
CanESM5-ISIMIP3b-hist	-0.31	3.67	0.52	-0.55	388	1009	0.006	0.23	0.1	0.123	-0.009	0.001	0.006	Bias Adjustment and Nitrogen Cycle
CanESM5-ISIMIP3b-NCycle-hist	0.48	4.95	0.69	-0.15	300	847	0.01	0.297	0.108	0.179	-0.01	0.001	0.006	
CanESM5-ISIMIP3b-NCycleV2-hist	0.78	7.39	0.98	-0.32	344	1299	0.02	0.34	0.126	0.194	-0.016	0.001	0.007	
CanESM5-ISIMIP3b-SSP585	3.43	6.64	3.6	0.22	586	981	0.016	0.647	0.29	0.341	-0.001	0	-0.005	
CanESM5-ISIMIP3b-NCycle-SSP585	0.73	4.18	1.73	-0.2	414	822	-0.023	0.5	0.24	0.284	-0.002	0	-0.005	
CanESM5-ISIMIP3b-NCycleV2-SSP585	1.74	6.92	2.82	-0.22	534	1271	-0.027	0.57	0.254	0.344	-0.004	0	-0.004	

Flux (PgC yr-1)
8 6 4 2 0 -2 -4 -6 -8
Stock (PgC)
1600 1400 1200 1000 800 600 400 200
Trend in flux (PgC yr-2)
0.8 0.6 0.4 0.2 0 -0.2 -0.4 -0.6 -0.8

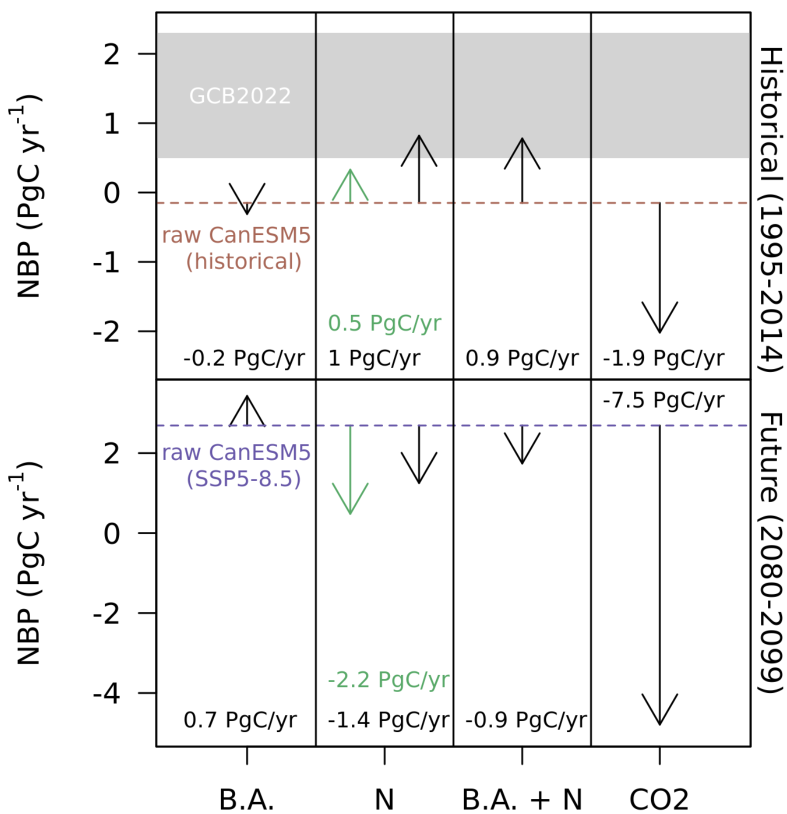

GCB2022
raw CanESM5
(historical)
raw CanESM5
(SSP5-8.5)
NBP (PgC yr-1)
-0.2 PgC/yr
0.5 PgC/yr
1 PgC/yr
0.9 PgC/yr
-1.9 PgC/yr
-7.5 PgC/yr
0.7 PgC/yr
-2.2 PgC/yr
-1.4 PgC/yr
-0.9 PgC/yr
Historical (1995-2014)
Future (2080-2099)
B.A.
N
B.A. + N
CO2

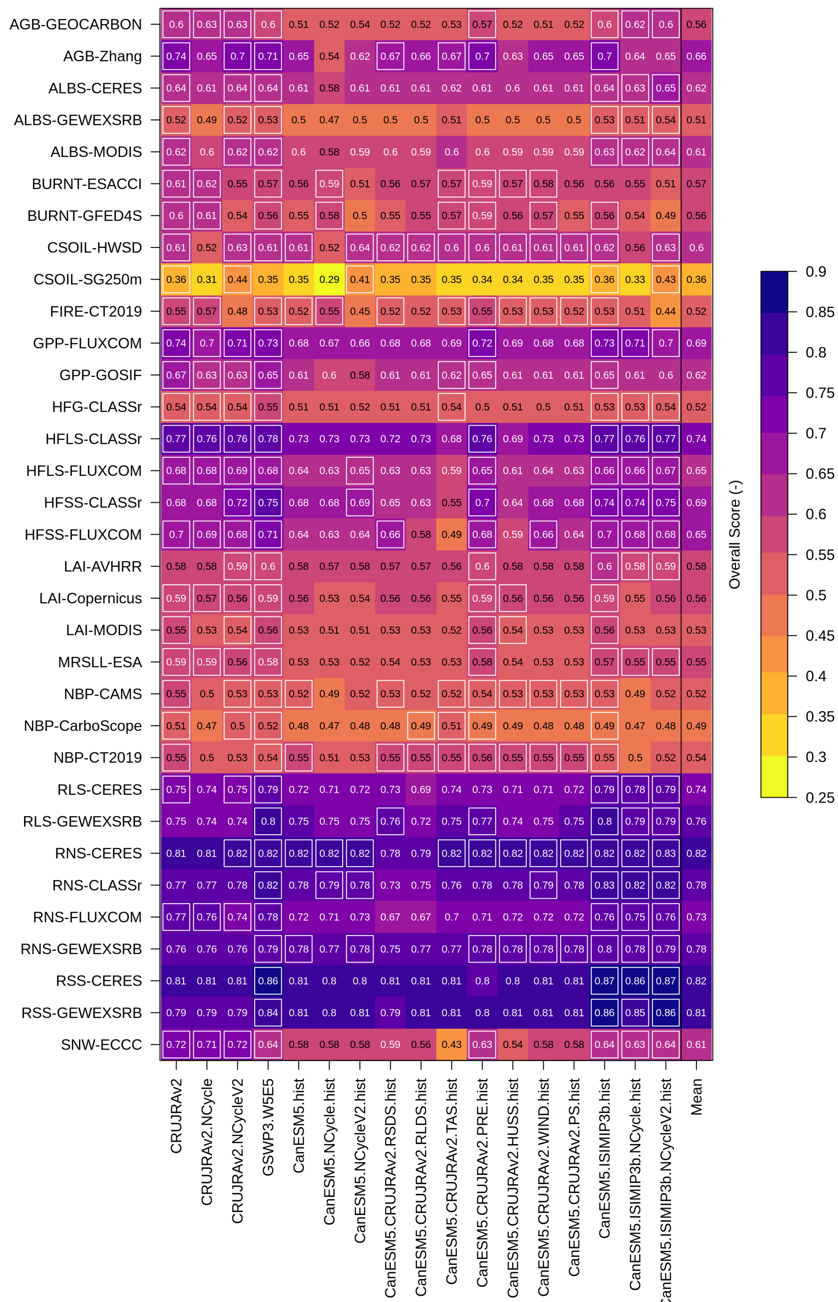
AGB-GEOCARBON
AGB-Zhang
ALBS-CERES
ALBS-GEWEXSRB
ALBS-MODIS
BURNT-ESACCI
BURNT-GFED4S
CSOIL-HWSD
CSOIL-SG250m
FIRE-CT2019
GPP-FLUXCOM
GPP-GOSIF
HFG-CLASSr
HFLS-CLASSr
HFLS-FLUXCOM
HFSS-CLASSr
HFSS-FLUXCOM
LAI-AVHRR
LAI-Copernicus
LAI-MODIS
MRSLL-ESA
NBP-CAMS
NBP-CarboScope
NBP-CT2019
RLS-CERES
RLS-GEWEXSRB
RNS-CERES
RNS-CLASSr
RNS-FLUXCOM
RNS-GEWEXSRB
RSS-CERES
RSS-GEWEXSRB
SNW-ECCC
CRUJRAv2
CRUJRAv2.NCycle
CRUJRAv2.NCycleV2
GSWP3.W5E5
CanESM5.hist
CanESM5.NCycle.hist
CanESM5.NCycleV2.hist
CanESM5.CRUJRAv2.RSDS.hist
CanESM5.CRUJRAv2.RLDS.hist
CanESM5.CRUJRAv2.TAS.hist
CanESM5.CRUJRAv2.PRE.hist
CanESM5.CRUJRAv2.HUSS.hist
CanESM5.CRUJRAv2.WIND.hist
CanESM5.CRUJRAv2.PS.hist
CanESM5.ISIMIP3b.hist
CanESM5.ISIMIP3b.NCycle.hist
CanESM5.ISIMIP3b.NCycleV2.hist
Mean
Overall Score (-)
0.9
0.85
0.8
0.75
0.7
0.65
0.6
0.55
0.5
0.45
0.4
0.35
0.3
0.25

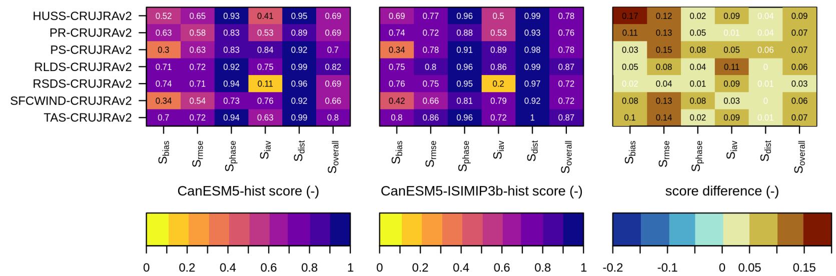
HUSS-CRUJRAv2
PR-CRUJRAv2
PS-CRUJRAv2
RLDS-CRUJRAv2
RSDS-CRUJRAv2
SFCWIND-CRUJRAv2
TAS-CRUJRAv2
S_{bias} S_{rmse} S_{phase} S_{av} S_{dist} $S_{overall}$
CanESM5-hist score (-)
CanESM5-ISIMIP3b-hist score (-)
score difference (-)
0 0.2 0.4 0.6 0.8 1
0 0.2 0.4 0.6 0.8 1
-0.2 -0.1 0 0.05 0.15

The Impact of Climate Forcing Biases and the Nitrogen Cycle on Land Carbon Balance Projections

Christian Seiler[1,2], Sian Kou-Giesbrecht[3], Vivek K. Arora[3], Joe R. Melton[1]

[1]Climate Processes Section, Climate Research Division, Environment and Climate Change Canada, Victoria, Canada
[2]School of Environmental Studies, Queen's University, Kingston, Canada
[3]Canadian Centre for Climate Modelling and Analysis, Climate Research Division, Environment and Climate Change Canada, Victoria, Canada

Key Points:

- Bias adjustment improves model performance across most ecosystem variables primarily due to reduced biases in precipitation.
- The inclusion of the N cycle increases the C sink during the historical period, placing it within the observed uncertainty range.
- The future C sink increases with bias adjustment and decreases with the N cycle, resulting in a net decrease when both factors are at play.

Corresponding author: Christian Seiler, `christian.seiler@queensu.ca`

Abstract

Earth System Models (ESMs) project that the terrestrial carbon sink will continue to grow as atmospheric CO_2 increases, but this projection is uncertain due to biases in the simulated climate and how ESMs represent ecosystem processes. In particular, the strength of the CO_2 fertilization effect, which is modulated by nutrient cycles, varies substantially across models. This study evaluates land carbon balance uncertainties for the Canadian Earth System Model (CanESM) by conducting simulations where the latest version of CanESM's land surface component is driven offline with raw and bias-adjusted CanESM5 climate forcing data. To quantify the impact of nutrient limitation, we complete simulations where the nitrogen cycle is enabled or disabled. Results show that bias adjustment improves model performance across most ecosystem variables, primarily due to reduced biases in precipitation. Turning the nitrogen cycle on increases the global land carbon sink during the historical period (1995-2014) due to enhanced nitrogen deposition, placing it within the Global Carbon Budget uncertainty range. During the future period (2080-2099), the simulated land carbon sink increases in response to bias adjustment and decreases in response to the dynamic carbon-nitrogen interaction, leading to a net decrease when both factors are acting together. The dominating impact of the nitrogen cycle demonstrates the importance of representing nutrient limitation in ESMs. Such efforts may produce more robust carbon balance projections in support of global climate change mitigation policies such as the 2015 Paris Agreement.

Plain Language Summary

The implementation of global climate change policies relies on our ability to predict how the global carbon cycle will evolve in the future. Climate models project that the biosphere will continue to absorb more CO_2 than it emits, keeping atmospheric CO_2 levels lower than they would be otherwise. However, the strength of this net CO_2 uptake varies considerably among models. This is because of differences in the simulated climate as well as the use of different methods for simulating plant growth. This study evaluates the importance of both factors by running one model with different climate data sets and model configurations. Our results show that the future net CO_2 uptake by plants increases when removing biases in climatic conditions and decreases when accounting for the impact of soil nutrients on plant growth, leading to a net decrease when both factors are acting together. The dominating impact of the nutrients demonstrates the importance of representing nutrient limitation in climate models. Such efforts may produce more robust carbon balance projections in support of global climate change mitigation policies such as the 2015 Paris Agreement.

1 Introduction

The 2015 Paris Agreement is a legally binding international treaty designed to limit global warming to well below 2°C, preferably to 1.5°C, compared to pre-industrial levels (UNFCCC, 2015). To reach this goal, global net anthropogenic carbon dioxide (CO_2) emissions must decline by about 45% from 2010 levels by 2030, reaching net-zero around 2050 (Rogelj et al., 2018). Such mitigation measures are based on our understanding of how the terrestrial carbon cycle responds to anthropogenic CO_2 emissions and associated changes in climate.

The terrestrial biosphere currently absorbs about one-third of total anthropogenic CO_2 emission (Friedlingstein et al., 2022). Earth System Models (ESMs) that participate in the Coupled Model Intercomparison Project Phase 6 (CMIP6) project that the terrestrial carbon sink continues to increase in the future, but that the fraction of anthropogenic CO_2 emissions absorbed by the terrestrial biosphere declines as emissions continue to grow (Canadell et al., 2021). Such carbon cycle projections, however, have very large uncertainties, ranging from about 2 to 7 PgC per year for the projected land sink towards the end of the 21st century under the Shared Socioeconomic Pathway SSP5-8.5.

The large inter-model spread may be due to a variety of reasons, including variations among ESMs in their representations of key processes. For instance, out of the eleven ESMs assessed in Canadell et al. (2021), only six include an interactive terrestrial nitrogen cycle, five account for forest fires, three allow for competition among Plant Functional Types (PFTs), and only two represent carbon dynamics in permafrost. According to Arora et al. (2020), CMIP6 ESMs that take into account dynamic terrestrial carbon-nitrogen interaction take up less carbon than those without a terrestrial nitrogen cycle representation in response to future increases in atmospheric [CO_2]. The same study found that the variability in feedback parameters, which represent the interactions between climate and the carbon cycle, is less in ESMs that include the terrestrial nitrogen cycle. This finding suggests that the inter-model spread of carbon balance projections could decrease if all ESMs would account for the limiting impacts of nutrients on plant growth.

Another source of uncertainty is the sensitivity of carbon cycle projections to biases in the meteorological forcing. Model performance has generally improved from CMIP5 to CMIP6 (Eyring et al., 2021) in reproducing observed climatic variables. While the multi-model mean captures most aspects of the observed climate change well, biases can be substantial for individual models. For instance, biases in the annual mean surface temperature of individual CMIP6 models range between -7.5°C (e.g. FGOALS-g3 in northern Eurasia) and +7.5°C (e.g. MIROC6 in eastern Siberia) (Fan et al., 2020). Similarly, while the CMIP6 multi-model mean captures the observed global mean surface temperature trend well, trends from individual models can deviate substantially from observations. In the case of the Canadian Earth System Model version 5 (CanESM5), warming trends computed from 1981 to 2014 are about twice the observed rate over this period, possibly due to its larger-than-observed climate sensitivity (Swart et al., 2019).

One approach for assessing the impact of biases in climate forcing on future projections is to adjust the model data for biases present in the historical period, under the assumption that these biases are stationary between the historical and future periods. To test this stationarity assumption, Krinner et al. (2020) bias-adjusted a climate model for the historical and future period using data from another climate model rather than observations as a reference. The authors then compared the differences between the bias-adjusted data and the reference climate model data for the historical and future periods and concluded that biases are indeed stationary. This suggests that bias-adjusting the future climate model projections on the basis of historical biases is a valid approach.

To evaluate the impact of climate forcing biases on terrestrial carbon cycle projections, Ahlström et al. (2017) forced a terrestrial ecosystem model (LPJ-GUESS) with raw and bias-adjusted temperature, precipitation, and incoming shortwave radiation data provided by 15 models that form part of CMIP Phase 5 (CMIP5). Their study shows that bias adjustment reduces the ensemble's spread of ecosystem carbon during the 1850-2100 period to about 20% of the ensemble's original range. The projected ecosystem carbon change from the 1996-2005 period to the 2091-2100 period was also affected by bias adjustment, reducing the ensemble's original range of carbon uptake to about 60% of the ensemble's original range. Note that the change in ecosystem carbon corresponds to net biome productivity (NBP), where positive values represent a carbon sink while negative values represent a carbon source. The authors conclude that climate biases play a major role in CMIP5 terrestrial carbon cycle simulations, with a larger impact on the carbon pool sizes than on their changes in time.

Padrón et al. (2022) on the other hand, show that the primary factors contributing to projected NBP uncertainty of CMIP6 ESMs are the response of the land carbon cycle to temperature and soil moisture variability, followed by the sensitivity of NBP to atmospheric carbon dioxide concentration ([CO_2], hereafter). Using multiple linear regression and a resampling technique, the authors show that the influence of average climate conditions is considerably less compared to the factors listed above, indicating that biases in climate models may have only a moderate impact on uncertainties in land carbon balance projections.

The relation between biases in the climate forcing, nutrient cycles, and land carbon balance projections can be thought of as follows. Carbon cycle simulations conducted online with ESMs or offline with land models are based on a spinup followed by a transient run. During the spinup, a land surface model is forced with meteorological data that mimic pre-industrial conditions. All other forcing data, such as [CO_2] or nitrogen deposition, are set to constant values representative of pre-industrial times. The model is run until all carbon fluxes are in equilibrium with the environment, implying that NBP is close to zero. The spinup is followed by a transient run where all forcings evolve in time. The trends of the forcings then push the model into a non-equilibrium state, such that NBP starts to differ from zero, where positive values represent a carbon sink and negative values a carbon source.

From this perspective, biases in the mean climate state are irrelevant, since NBP is driven by the trends in climate forcing. However, biases in the mean climate state may affect NBP nevertheless, because of the non-linear relationship between carbon fluxes and a given forcing. For instance, net primary productivity (NPP) increases with increasing temperature until it reaches a temperature optimum, after which NPP declines (Figure 1a). The model's sensitivity to a trend of a given forcing, therefore, depends on the mean climate state. Furthermore, the relation between NPP and temperature changes if dynamic carbon-nitrogen coupling is enabled, implying that the impact of biases in the mean state depends on whether the nitrogen cycle is turned on or off (Figure 1b). Finally, the impact of the nitrogen cycle may also vary depending on the exact choice of parameter values.

The extent to which NBP projections are affected by climate model biases versus nutrient limitation remains unclear and may vary considerably among models. The goal of our paper is to evaluate the impact of both drivers using the Canadian Earth System Model (CanESM) as a case study. To achieve this we conduct simulations where the latest version of the CanESM land surface component is run offline with quasi-observed data, raw CanESM5 climate data, and bias-adjusted CanESM5 data. Contrary to the study by Ahlström et al. (2017) we adopted a more consistent experimental design where offline and online runs are based on the same land surface model, with the restriction that the offline model version is more advanced to allow for dynamic carbon-nitrogen interaction. Furthermore, we conducted a wide range of control experiments (26 in total) that allow us to explore our results in greater depth. Our main research questions are:

- How do bias adjustment and the nitrogen cycle affect model performance across ecosystem variables, and which meteorological forcing variables deteriorate model performance most?
- What are the relative impacts of bias adjustment and the nitrogen cycle for land carbon balance projections?
- How sensitive are our results to different nitrogen cycle parameter values?

The answers to these questions provide insights that contribute to preparation of the land component of CanESM for the upcoming CMIP Phase 7 and support our efforts to minimize uncertainties in carbon cycle projections. In the following, the Methods section describes the forcing data sets, experimental protocol, the CanESM land surface component employed here, and the statistical framework used for quantifying model performance. The results section documents how bias adjustment, nitrogen cycle, and both factors combined affect model performance and carbon cycle projections. The discussion section elaborates on the main findings with a particular focus on the potential impacts of future model development on carbon cycle projections.

2 Methods

2.1 Meteorological forcing data sets

The present study is based on a range of simulations where the latest version of the CanESM land surface component is forced offline with four different meteorological data sets. The first two meteorological data sets present quasi-observed values, which are (i) the blended Climate Research Unit - Japanese 55-year Reanalysis version 2.0 product (CRUJRAv2; 1901-2014; Harris et al. (2014); Kobayashi et al. (2015)) and (ii) the Global Soil Wetness Project Phase 3 (GSWP3) - WFDE5 over land merged with ERA5 over the ocean (W5E5) (GSWP3-W5E5; 1901-2014; Cucchi et al. (2020)). The third data set presents meteorological forcing generated by CanESM5 (Swart et al., 2019), and the fourth data set is the bias-adjusted version of the CanESM5 meteorological forcing provided by phase 3b of the Inter-Sectoral Impact Model Intercomparison Project, referred to as ISIMIP3b, hereafter (Lange, 2019).

The bias adjustment is based on a parametric quantile mapping method that has been designed to robustly adjust biases in all percentiles of a distribution and to preserve trends in these percentiles (Lange, 2019). The corresponding bias adjustment target is the quasi-observed GSWP3-W5E5 dataset mentioned previously. Therefore, CRUJRAv2 serves as our primary source of reference as it is independent of the bias-adjusted CanESM5 data. Additional analysis with a GSWP3-W5E5-driven simulation enables us to evaluate whether differences between model output and observation-based reference data, such as remotely sensed gross primary productivity, are due to shortcomings in the bias adjustment technique or due to observational uncertainties. All meteorological forcings are disaggregated from 6-hourly to half-hourly time steps, following the methodology explained in Melton and Arora (2016). The bias-adjusted CanESM5 data are spatially interpolated to the same horizontal resolution as the parent CanESM5 data (T63; 128×64; 2.81°).

2.2 Experimental Protocol

All simulations consist of a pre-industrial spinup period followed by a transient simulation. CLASSIC is spun up until the terrestrial carbon cycle is in equilibrium with all forcing data including a prescribed [CO_2]. This requires that all time-varying input variables other than the meteorological forcing are kept constant, which includes [CO_2], land cover, population density, lightning, and nitrogen deposition and fertilization, if applicable. The constant value corresponds to the value for the first year of the transient run. The duration of the spinup is 500 years when the nitrogen cycle is turned off and 2300 years when the nitrogen cycle is turned on (Table 1). Once model pools are in equilibrium, the model enters the transient run where [CO_2], land cover, population density, nitrogen deposition and nitrogen fertilization (if applicable) vary in time. Since lightning data are not available before 1990s, climatological monthly lightning (used in the fire module) is used for all years. The starting year of the transient run varies among simulations, with 1901 for CRUJRAv2 and GSWP3-W5E5, and 1850 for CanESM5 and ISIMIP3b. Historical simulations end in 2014, while the Shared Socioeconomic Pathway SSP5-8.5 projections span the period from 2015 to 2099 (Table 1).

We conducted a total of 26 simulations for evaluating the impact of climate forcing biases and the nitrogen cycle on carbon cycle dynamics (Table 2). Each simulation has been spun up until carbon fluxes reached equilibrium with their environment (Table 1). For the first four simulations listed in Table 2, we force CLASSIC with CRUJRAv2, GSWP3-W5E5, CanESM5, and bias-adjusted CanESM5, here referred to as ISIMIP3b, meteorological data. These simulations were completed for the historical period with the nitrogen cycle turned off. To identify what variables in CanESM5 deteriorate model performance most we ran seven additional experiments where we replaced one meteorological variable at a time from CanESM5 with the corresponding data from CRUJRAv2. For instance, the simulation CanESM5-CRUJRAv2.TAS-hist is based on CanESM5 forcing, except for near-surface air temperature, which has been replaced with values from CRUJRAv2. The next two simulations listed in Table 2 (CanESM5-SSP5-8.5 and CanESM5-ISIMIP3b-SSP5-8.5) show how bias adjustment affects future projections of carbon dynamics for the period 2015-2099 when the nitrogen cycle is turned off. The following four simulations listed in Table 2 assess the sensitivity of carbon dynamics to dynamic nitrogen coupling using the default nitrogen cycle parameter values. The next set of four simulations are identical to the previous simulations, except that they are based on a different set of nitrogen cycle parameter values (see section 2.4 for details). The last three simulations are used to compare the impact of increasing [CO_2] versus changes in climate on carbon dynamics under current and future climate conditions.

2.3 Reference Data

We evaluate model performance for 16 ecosystem variables using 33 globally gridded observation-based reference data sets (Table 3). The respective variables are net surface radiation (RNS), net shortwave (SW) radiation (RSS), net longwave (LW) radiation (RLS), surface albedo (ALBS), leaf area index (LAI), gross primary productivity (GPP), net biome productivity (NBP), emissions from fires (FIRE), fractional area burnt (BURNT), above-ground biomass (AGB), soil organic carbon (CSOIL), latent heat flux (HFLS), sensible heat flux (HFSS), soil heat flux (HFG), soil moisture (MRSLL), and snow water equivalent (SNW). NBP is defined as GPP minus RECO minus fluxes associated with disturbances such as wildfires and land use change. Another variable discussed in the results section is net ecosystem productivity (NEP), which is defined as GPP minus RECO. Details on each data set are provided by Seiler et al. (2021) and Seiler et al. (2022).

2.4 Canadian Land Surface Scheme Including Biogeochemical Cycles (CLASSIC)

The simulations presented here are conducted with the Canadian Land Surface Scheme Including Biogeochemical Cycles (CLASSIC) (Melton et al., 2020). CLASSIC, formally known as CLASS-CTEM, forms the land surface component of the Canadian Earth System Model (CanESM) (Swart et al., 2019). The model configuration used here considers five carbon pools (leaves, stem, roots, litter, and soil) and nine Plant Functional Types (PFTs) (needleleaf evergreen, needleleaf deciduous, broadleaf evergreen, broadleaf cold deciduous, broadleaf drought/dry deciduous, C3 Grass, C4 Grass, C3 Crop, and C4 Crop). Model inputs that vary in time include seven meteorological variables (downwelling SW radiation, downwelling LW radiation, surface precipitation rate, surface air pressure, specific humidity, air temperature, and wind speed), [CO_2], land cover, and population density. Another input variable is lightning density, which is based on climatological monthly values. The main processes simulated by the biogeochemical component of CLASSIC include photosynthesis, canopy conductance, tissue turnover, allocation of carbon, and phenology (Arora & Boer, 2005b), dynamic root distribution (Arora & Boer, 2003), maintenance, growth and heterotrophic respiration (Melton et al., 2015), wildfires (Arora & Boer, 2005a; Arora & Melton, 2018), land use change (Arora & Boer, 2010), and nitrogen cycle (Asaadi & Arora, 2021; Kou-Giesbrecht & Arora, 2022b). The land carbon balance depends on how carbon fluxes respond to changes in environmental conditions and land use change. Of particular importance is how GPP and respiration respond to changes in temperature, precipitation, and [CO_2]. Those dependencies are summarized next, with more details provided in the Supplementary Information (Text S1-6 and Figure S1).

The representation of photosynthesis is based on the parameterization by Farquhar et al. (1980) and Collatz et al. (1991, 1992). The Farquhar photosynthesis scheme estimates the gross leaf photosynthesis rate, G_o (mol CO_2 m^{-2} s^{-1}) as the minimum of three photosynthetic states: (1) the Rubisco-limited state (J_c), (2) the Ribulose 1,5-bisphosphate (RuBP)-limited state (J_e), and (3) the triose-phosphate utilization (TPU)-limited state (J_s). These photosynthetic states depend on four parameters that vary with temperature, namely the Michaelis-Menten constants for (i) CO_2 (K_c) and (ii) O_2 (K_o), (iii) the selectivity of Rubisco for CO_2 over O_2 (σ), and (iv) the maximum carboxylation rate (V_m). The temperature dependence of those four parameters is expressed through four different standard Q_{10} functions (Figure S1). Finally, J_e and J_c also depend on the partial pressure of CO_2 in the leaf interior, which is affected by [CO_2].

In CLASSIC, autotrophic respiration (R_a; mol CO_2 m^{-2} s^{-1}) equals the sum of maintenance respiration (R_m) and growth respiration (R_g). The maintenance respiration of a plant is the sum of the maintenance respiration for leaves, stems, and roots. Maintenance respiration varies with temperature following a Q_{10} function. For stems and roots, maintenance respiration also depends on PFT-specific base respiration rates. Growth respiration is modelled as a fraction of net primary productivity. Heterotrophic respiration (R_h; mol CO_2 m^{-2} s^{-1}) equals the sum of respiration from litter and soil organic carbon. Heterotrophic respiration rates depend on the size of their respective carbon pools, the availability of moisture, and temperature.

If the nitrogen cycle is turned off, V_m is computed from a PFT-specific carboxylation rate (V_{max}) and is adjusted for temperature and soil moisture (Figure 1c). If the nitrogen cycle is turned on, V_{max} is expressed as a function of leaf nitrogen content (N_L) (Figure 1d). We used two different sets of nitrogen cycle parameter values that differ with respect to the parameter values describing (i) the relationship between V_{max} and leaf nitrogen content (Γ_1), (ii) the dimensionless mineral nitrogen distribution coefficient used for calculating passive root uptake (β), and (iii) the efficiency of fine roots to take up nitrogen (ε) (Table S1). The default Γ_1 values were updated based on data provided by Kattge et al. (2009). The default β value was decreased while the default ε was increased to ensure that nitrogen uptake is dominated by active rather than passive uptake (Hopmans & Bristow, 2002). Using two different sets of parameter values allowed us to evaluate which of the two sets performs better when compared to observations and how sensitive carbon balance projections are to different nitrogen cycle parameter values. The relation between NPP, temperature, [CO_2], and leaf nitrogen content are illustrated in Figure 1.

2.5 Automated Model Benchmarking R package

The Automated Model Benchmarking R package developed by Seiler et al. (2022) quantifies model performance using a skill score system that is based on the International Land Model Benchmarking (ILAMB) framework (Collier et al., 2018). The method employs five scores that assess the model's annual mean bias (S_{bias}), monthly centralized root-mean-square-error (S_{rmse}), the timing of the seasonal peak (S_{phase}), inter-annual variability (S_{iav}), and spatial distribution (S_{dist}). The exact definition of each skill score is provided in the Supplementary Information. The main steps for computing a score usually include (i) computing a dimensionless statistical metric, (ii) scaling this metric onto a unit interval, and (iii) computing a spatial mean. All scores are dimensionless and range from zero to one, where increasing values imply better performance. These properties allow us to average skill scores across different statistical metrics in order to obtain an overall score for each variable ($S_{overall}$).

3 Results

3.1 Model performance

This section evaluates how model performance is affected by climate model biases, bias adjustment, and the nitrogen cycle by comparing AMBER scores among historical simulations. Comparing the raw CanESM5 forcing data (CanESM5-hist) and the bias-adjusted CanESM5 forcing data (CanESM5-ISIMIP3b-hist) against quasi-observed values from CRUJRAv2 shows that bias adjustment substantially improves scores across all seven meteorological forcing variables as well as all five statistical metrics (Figure 2). The largest improvements are generally found for the bias score and centralized root-mean-square error score. Bias adjustment substantially reduces the major temperature and precipitation biases, including a dry and warm bias in the Amazon basin, a wet bias in equatorial Africa, a warm bias in Eastern Siberia, and a cold bias in the Tibetan Plateau (Figure 3 a-b and e-f). Bias adjusting the meteorological forcing data translates into better model performance, as explained next.

For the vast majority of ecosystem variables, model performance is considerably worse when forcing CLASSIC with raw CanESM5 rather than quasi-observed values from either CRUJRAv2 or GSWP3-W5E5 (Figure 4). The only exceptions are net SW radiation, net LW radiation, and the resulting net surface radiation. Control experiments show that the poor model performance is mainly due to biases in precipitation (CanESM5.CRUJRAv2.PRE.hist vs. CanESM5.hist). Bias adjustment substantially improves model scores across almost all ecosystem variables (CanESM5-ISIMIP3b-hist vs.CanESM5-hist). Despite the widespread improvement, bias adjustment has no statistically significant impact on the model's ability to reproduce NBP. The reason for this is that NBP is affected not just by the average climate conditions but also by the trends in the climate forcing, in particular temperature trends, which remain unaffected by the bias adjustment technique.

Turning the nitrogen cycle on generally causes a statistically significant (5%-level) reduction of model performance, including the model's ability to reproduce NBP. This applies to simulations driven with CRUJRAv2, raw CanESM5 data, and bias-adjusted CanESM5 data. However, in the CanESM5-driven runs (raw and bias-adjusted), the nitrogen cycle causes global total NBP to be larger and thereby more consistent with estimates provided by the 2022 Global Carbon Budget (1.4 $\pm$ 0.9 PgC yr^{-1} during the 2000s; Friedlingstein et al. (2022)) (Figure 5). Updating the nitrogen parameter values (NcycleV2) generally improves scores compared to simulations that are based on the default values, in particular for soil organic carbon (Figure 4). The model's ability to reproduce wildfires (i.e. fractional area burnt and emissions from fires), on the other hand, worsens in response to the updated nitrogen parameter values. Again, this pattern applies to simulations driven by CRUJRAv2, raw CanESM5, and bias-adjusted CanESM5 data alike.

3.2 Land carbon balance

3.2.1 Without nitrogen cycle

This section explores the sensitivity of the land carbon balance to climate model biases and bias adjustment under historical and future climate conditions. The annual mean values reported here are computed for the last 20 years of a given simulation (1995-2014 for the historical simulation and 2080-2099 for the SSP5-8.5 scenario), while trends are computed for the last 50 years of a given simulation (1965-2014 for historical and 2050-2099 for SSP5-8.5). The trend is determined through linear regression and is based on a longer time period to reduce the impact of inter-annual variability.

Forcing CLASSIC with CRUJRAv2 and transient [CO_2] leads to an annual mean carbon sink of 1.74 PgC yr^{-1} during the 1995-2014 period (Figure 6; CRUJRAv2). This result is comparable to estimates provided by the 2022 Global Carbon Budget (1.4 $\pm$ 0.9 PgC yr^{-1} during the 2000s; Friedlingstein et al. (2022)). The carbon sink is driven by a positive GPP trend of 0.27 PgC yr^{-2} during the 1965-2014 period, which exceeds the positive trends in autotrophic and heterotrophic respiration during the same period (0.10 and 0.14 PgC yr^{-2}, respectively; Figure 6; CRUJRAv2). Trends in emissions from fires are negative, mainly due to an increase in population density and crop area over the historical period (Arora & Melton, 2018). Trends related to land use change emissions during the 1965-2014 period are an order of magnitude smaller compared to trends in net ecosystem productivity (NEP). Assessing the trends of the carbon pools shows that the vegetation acts as a carbon sink (1.03 PgC yr^{-1}), while the soil acts as a weak carbon source (-0.08 PgC yr^{-1}). The corresponding vegetation and soil organic carbon pools are 520 and 1130 PgC, respectively, which is within the uncertainty range of observation-based reference data (Seiler et al., 2022). As a comparison, the 2022 Global Carbon Budget reports a vegetation pool of 450 PgC and a soil organic carbon pool of 1700 PgC soil (Friedlingstein et al., 2022).

To assess whether the sink in the CRUJRAv2 simulation is driven by trends in [CO_2] or climate we conduct a counter-factual control experiment where [CO_2] is kept constant at the year 1700 concentrations (276.59 ppmv). Results show that while GPP, autotrophic respiration, and heterotrophic respiration all benefit from climate trends, the increase in GPP is weaker compared to the increase in ecosystem respiration, causing NEP to decline. As a result, NBP is negative (-0.94 PgC yr^{-1}; Figure 6; CRUJRAv2-CO2fixed) and vegetation and soil both act as a carbon source (-0.22 and -0.71 PgC yr^{-1} for vegetation and soil pool, respectively). The vegetation and soil organic carbon pool are therefore smaller compared to the CRUJRAv2 simulation (411 and 1050 PgC for vegetation and soil, respectively). Further analysis shows that the boreal zone is the only region that acts as a carbon sink when [CO_2] is kept constant at its pre-industrial level (not shown). The following sections describe how [CO_2], bias adjustment, and the nitrogen cycle affect NBP for simulations that are driven with CanESM5 data. The impacts are summarized in Figure 5 with more detail provided in Figure 6.

Forcing CLASSIC with CanESM5-hist data causes the land carbon balance to be almost carbon-neutral during the 1995-2014 period (NBP = -0.15 PgC yr^{-1}; Figure 5 and 6; CanESM5-hist). The reason for the almost carbon-neutral balance is that the CanESM5-hist simulation shows a much less pronounced increase in GPP compared to the CRUJRAv2 simulation. Consequently, the NEP values for the CanESM5-hist simulation are lower than those for the CRUJRAv2 simulations (3.69 and 4.76 PgC yr^{-1}, respectively; Figure 6). Trends in carbon pools are positive for vegetation and negative for soil, almost balancing each other (0.51 and -0.49 PgC yr^{-1}, respectively; Figure 6). The resulting carbon stocks of the vegetation and soil pools are considerably lower than the ones in the CRUJRAv2 simulation (360 and 968 PgC for vegetation and soil in CanESM5-hist, respectively). The almost carbon-neutral balance is driven by an underestimation of NBP in the boreal and temperate regions of Eurasia when compared to the simulation driven by CRUJRAv2 meteorological data (Figure 7g, h). A counter-factual control experiment where [CO_2] is kept constant at its pre-industrial level (276.59 ppmv) confirms that climate trends produced by CanESM5 have a negative impact on the land carbon balance (NBP = -2.02 PgC yr^{-1}) because the positive trend in heterotrophic respiration exceeds the positive trend in GPP (Figure 5 and 6; CanESM5-CO2fixed-hist and Figure).

To identify what variables cause the almost carbon-neutral balance in the CanESM5-hist simulation we conducted seven experiments where we replaced each of the seven CanESM5 meteorological forcing variables with data from CRUJRAv2 one at a time. Results show that the weak carbon source in the CanESM5-hist simulation was primarily driven by trends in temperature, followed by incoming LW radiation and precipitation (Table S2). Replacing CanESM5 with CRUJRAv2 near-surface temperature leads to a weak carbon sink of 0.55 PgC yr^{-1} (Figure 6; CanESM5-CRUJRAv2.TAS-hist). The large impact of temperature is likely due to the larger-than-observed warming trend during the historical period produced by CanESM5 (Swart et al., 2019).

Forcing CLASSIC with CanESM5-SSP5-8.5 leads to a carbon sink of 2.69 PgC yr^{-1} by the end of this century (Figure 5 and 6). This sink is driven by a strong increase in GPP that exceeds the increase in respiration. The vegetation carbon pool responds with a strong positive trend (2.88 PgC yr^{-1}), while the soil organic carbon pool exhibits a weak positive trend (0.01 PgC yr^{-1}). The sink is mainly located in the boreal regions of North America and Eurasia, as well as the Eurasia temperature zone (Figure 7 a, g and h). A control experiment where [CO_2] is kept at a constant level corresponding to the year 2014 (397.2 ppmv) yields a large carbon source by the end of this century, confirming that the sink in CanESM5-SSP5-8.5 is driven by trends in [CO_2] rather than climate (-4.79 PgC yr^{-1}; Figure 5 and 6; CanESM5-CO2fixed-SSP5-8.5). Although the terrestrial biosphere is simulated to act as a net carbon sink as a whole under SSP5-8.5, the model also simulates net sources on a regional scale. This applies in particular to the Amazon basin (Figure 8e), where precipitation is projected to decline (Figure 3g). This regional carbon source is more evident when using bias-adjusted forcing data, as explained next.

During the historical period, adjusting the CanESM5 forcing data for biases has only minor impacts on the carbon balance. However, these impacts become more pronounced during the future period. Under SSP5-8.5, bias adjustment causes NBP to be 28% larger compared to the non-bias adjusted simulation (Figure 6, comparing CanESM5-ISIMIP3b-SSP5-8.5 against CanESM5-SSP5-8.5 and Figure 5). Bias adjustment favours GPP more than it favours respiration, resulting in more NEP and stronger positive trends in the vegetation and soil organic carbon pools. The tendency for larger NBP values in the bias-adjusted simulation is most evident in North American boreal and temperate regions, as well as Tropical Asia (Figure 7 and 8). Compared to the simulation that is driven with raw CanESM5 forcing data, bias adjustment also enhances the projected carbon source in the Amazon basin (Figure 8e and g). Recall that bias adjustment mainly affects the absolute values of the forcing while the projected changes are largely preserved (Figure 3c-d, g-h and Figure S2). Therefore, the effects of bias correction stem from the fact that the sensitivity of the carbon cycle to a given forcing trend depends on its average state (Figure 1). In the case of the Amazon basin, bias adjustment reduces the dry bias and thereby enhances vegetation carbon. The projected decline in Amazonian precipitation then causes greater carbon emissions in the bias-adjusted simulation as there is more biomass available for burning and decomposition (Figure S3 and S4).

3.2.2 With nitrogen cycle

The impact of the nitrogen cycle varies among simulations and the selection of parameter values. In the case of simulations with CRUJRAv2 forcing, the nitrogen cycle in its default configuration leads to a weaker carbon sink compared to when the nitrogen cycle is turned off (Figure 6; CRUJRAv2-NCycle vs CRUJRAv2). This is because the nitrogen cycle causes a weaker increase in GPP and a stronger increase in heterotrophic respiration compared to the corresponding simulation without the nitrogen cycle. As a result, the positive vegetation carbon trend becomes weaker and the vegetation and soil organic carbon pools are considerably smaller.

Using the updated nitrogen cycle parameter values increases the carbon sink such that it exceeds the NBP from the CRUJRAv2 simulation, which is due to a stronger increase in GPP (Figure 5 and 6; CRUJRAv2-NCycleV2). The trend in vegetation carbon increases more strongly and the soil becomes a carbon sink as the carbon flux from the vegetation to the soil pool increases, outpacing the losses due to heterotrophic respiration. The different responses are caused by differences in parameter values, where the updated values enhance active root nitrogen uptake.

Simulations that are driven with CanESM5-hist data show that both nitrogen cycle parameter value sets enhance NBP during the historical period compared to the corresponding simulation when the nitrogen cycle is turned off (Figure 6; CanESM5-NCycle-hist and CanESM5-NCycleV2-hist vs CanESM5-hist). Comparing the simulations that are based on the default and the updated nitrogen cycle parameter values shows that the latter yields larger values in NBP (0.33 and 0.82 PgC yr^{-1} for CanESM5-NCycle-hist and CanESM5-NCycleV2-hist, respectively). In both cases, the vegetation carbon pool acts as a sink while the soil carbon pool acts as a source. The NBP in the boreal regions of North America and Eurasia, as well as temperate Eurasia, benefit most from the nitrogen cycle (Figure 7 and 8).

For future projections, both nitrogen cycle parameterizations reduce the increase in NBP compared to the corresponding simulation when the nitrogen cycle is turned off (54% less when using the updated nitrogen cycle parameter values) (Figure 5 and 6; CanESM5-NCycleV2-SSP5-8.5 vs CanESM5-SSP5-8.5). The impact of the nitrogen cycle is most evident in the boreal regions of North America and Eurasia, temperature Eurasia, Africa, and tropical Asia (Figure 7). In the Amazon basin, the nitrogen cycle diminishes the reduction of NBP, which reduces the projected loss of vegetation carbon (Figure 8 and S4). The reason for this is that the dynamic carbon-nitrogen coupling results in less biomass buildup in the Amazon compared to when the nitrogen cycle is deactivated, causing the projected loss in biomass to be lower as well.

The fact that the inclusion of the nitrogen cycle enhances the NBP increase during the historical period and reduces the NBP increase under SSP5-8.5 is consistent with how prescribed nitrogen inputs vary in time. Nitrogen fertilization and atmospheric deposition increase during the historical period and are projected to remain approximately constant after 2030 for SSP5-8.5 (Figure 9). The combined impact of bias adjustment and nitrogen cycle is dominated by the impact of the nitrogen cycle, with more NBP during the historical period and less NBP under SSP5-8.5 (-35%) when compared to the CanESM5-hist and CanESM5-SSP5-8.5 simulations, respectively (Figure 5).

4 Discussion

This study examines how biases in the climate forcing affect land carbon balance projections when dynamic carbon-nitrogen interactions are turned on or off. Using raw and bias-adjusted CanESM5 meteorological data, we find that bias adjustment improves model performance considerably across a wide range of ecosystem variables. This improvement is primarily due to bias reduction in precipitation. In the case of NBP, however, the impacts of bias adjustment on model performance is modest. This result aligns with the idea that NBP is mainly influenced by the trend of a forcing factor, which remains unaffected by the bias adjustment technique. Simulations that are based on raw and bias-adjusted CanESM5 meteorological forcing data do not reproduce the historical land carbon sink as long as the nitrogen cycle is turned off. Control experiments show that this is due to the exaggerated warming trend present in CanESM5, which weakens GPP trends more than respiration trends. While the impact of bias adjustment on NBP is small during the historical period, it is considerably larger during the 2080-2099 period under SSP5-8.5, where NBP is 28% larger in the simulation that is based on the bias-adjusted CanESM5 forcing compared to the raw CanESM5 forcing when the nitrogen cycle is turned off. Note that an increase of NBP in response to bias adjustment may be an a-typical reaction, since the bias adjustment conducted by Ahlström et al. (2017) weakened NBP for the vast majority of CMIP5 models. This apparent contradiction may be related to differences in the two land surface models involved (i.e. CLASSIC versus LPJ-GUESS) and/or the particularities of CanESM5.

While the model performance is degraded when nitrogen cycle is turned on, its inclusion increases NBP such that the CanESM5-driven simulations reproduce the carbon sink over the historical period. This response is consistent with the prescribed increase of the nitrogen fertilization and deposition during the historical period. During the 2080-2099 period, on the other hand, the nitrogen cycle weakens the increase of NBP, such that NBP is 54% less compared to projections when the nitrogen cycle is turned off. The impact of the nitrogen cycle during the future period is consistent with how nutrient availability limits the CO_2 fertilization effect, confirming findings from previous studies (Zaehle et al., 2010; Huntzinger et al., 2017; Meyerholt et al., 2020; Kou-Giesbrecht & Arora, 2022a). Simulations where the nitrogen cycle and bias adjustment act together show that the impact on NBP is dominated by the nitrogen cycle rather than by bias adjustment, where projected NBP is 35% lower compared to simulations that are based on raw CanESM5 data and when the nitrogen cycle is turned off. In conclusion, our findings demonstrate that both climate model biases and the nitrogen cycle affect NBP projections considerably, with the latter having a more substantial impact.

Some biases in CanESM5, such as the dry bias in the Amazon basin or the cold bias in the Tibetan plateau, have existed for decades and may not be resolved before the upcoming Coupled Model Intercomparison Project Phase 7 (CMIP7) (Swart et al., 2019). To address those biases nevertheless, one could apply an online bias-adjustment approach where the atmospheric model is nudged to a time-varying reference state (Guldberg et al., 2005). Applying an online bias adjustment to an earlier version of CanESM (CanESM2), Krinner et al. (2020) showed that this technique improves model performance for a wide range of variables, including precipitation. Online bias adjustment could therefore present a feasible path toward producing more reliable climate and carbon cycle projections.

Over the past decade, CLASSIC has undergone significant advancements, with the incorporation of new processes that have been evaluated primarily offline. Some of these developments will enhance the capabilities of the CanESM version that will participate in CMIP7. A potential list of those processes includes the dynamic carbon-nitrogen interaction discussed here, wildfires (Arora & Boer, 2005a; Arora & Melton, 2018), PFT competition (Melton & Arora, 2016), shrubs (Meyer et al., 2021), and permafrost carbon physics and dynamics (Melton et al., 2019). Future capabilities that are currently under development and that are likely to impact carbon balance projections include dynamic tiling of land use and land cover change, representation of bryophytes, lateral hydrological flow, explicit representation of plant hydraulics, and an improved representation of wildfires in the boreal regions. Longer-term future development also includes the incorporation of a phosphorus cycle. Some of these processes and their relevance for carbon cycle projections are discussed next.

Carbon emissions from wildfires originate mostly from the tropics, with about half of all global emissions coming from Africa, one quarter from South America and 9% from Australia during the 1960-2000 period (Schultz et al., 2008). Carbon emissions from the temperate and boreal regions, on the other hand, contributed about 5% on average during the same period. In the last two decades, however, forest loss associated with wildfires has roughly doubled in Eurasia (Tyukavina et al., 2022). The interannual variability of boreal forest fires is to a large extent driven by the interannual variability of lightning, which is likely to increase with future warming and more convective precipitation (Veraverbeke et al., 2017). Wildfires in the boreal zone may, therefore, play an increasingly important role in the global carbon balance (Loehman, 2020). The CLASSIC version presented here is able to reproduce global total carbon emissions reasonably well but underestimates wildfire emissions in the boreal zone (Arora & Melton, 2018; F. Li et al., 2019; Seiler et al., 2021). Current model development efforts are working to improve the representation of boreal fires in CLASSIC to ensure that the model will be capable of projecting potential changes in future fire regimes. This could reverse the projected trend in wildfire emissions presented here and improve NBP projections.

The global carbon budget estimates that emissions from deforestation are approximately 1.8 (±0.4) PgC yr^{-1} during the 2012-2021 period (Friedlingstein et al., 2022). The corresponding value produced in the CRUJRAv2 simulation is considerably lower (0.69 PgC yr^{-1} for the 1995-2014 period when adding emissions from deforestation and the decomposition of wood products), possibly due to the following reason. In CLASSIC, deforestation occurs when natural vegetation is converted to croplands, while conversion to pasture area is not taken into account. Once the conversion to cropland takes place, the area remains cropland, until abandoned, and no regrowth can occur. Current model developments on dynamic tiling are expected to increase land use change emissions in the model bringing them closer to observation-based values from book-keeping models. It should be noted that neither the Global Carbon Budget (Friedlingstein et al., 2022) nor CLASSIC account for emissions associated with forest degradation.

The strength of the carbon sink in northern high latitudes is still a matter of debate, with various studies providing conflicting results (McGuire et al., 2012; Belshe et al., 2013; Schuur et al., 2022; Friedlingstein et al., 2022). Concerning the future, the vast majority of CMIP6 ESMs predict that the northern high latitudes will act as a net carbon sink under the SSP5-8.5 scenario (Canadell et al., 2021). However, since only two CMIP6 ESMs include a representation of permafrost carbon gradual thaw processes (Canadell et al., 2021), and none of the models represent abrupt thaw processes (Turetsky et al., 2020), such projections are subject to considerable uncertainty. Models explicitly designed for permafrost carbon cycle dynamics simulate a carbon release from the permafrost zone in response to global warming (Schneider von Deimling et al., 2015). Such models may overestimate the net release as they ignore the compensating effect of stimulated plant growth. To address this issue, the Permafrost Carbon Network organized a multi-model assessment with state-of-the-art land models that couple thaw depth with soil carbon exposure (McGuire et al., 2018). The study shows that four out of five models project a net carbon source, with a mean carbon loss of 208 PgC under a high-emission scenario (RCP8.5) by 2100. The permafrost carbon feedback is potentially so strong that it is included in the Intergovernmental Panel on Climate Change's estimate of the remaining carbon budget for climate stabilization (Canadell et al., 2021). While CLASSIC is well suited to simulate the physics of permafrost regions (Melton et al., 2019), the model version used here still lacks processes relevant for simulating permafrost carbon dynamics. However, the implementation of permafrost carbon processes in CLASSIC is in progress, using an approach presented by Koven et al. (2011). Accounting for permafrost carbon dynamics presents another potentially essential step toward more reliable carbon balance projections.

The model version examined in this study includes a representation of dynamic carbon-nitrogen interaction but ignores the limiting impact of phosphorus on photosynthesis (Elser et al., 2007; Vitousek et al., 2010; Reed et al., 2015). Model results from previous studies suggest that the strength of the projected land carbon sink is considerably lower when accounting for the limiting impact of nitrogen and phosphorus together (25% less compared to simulations without nitrogen or phosphorus cycling under the Special Report on Emissions Scenarios; Goll et al. (2012)). Longer-term model development will therefore consider the addition of a phosphorus cycle to fully account for the impact of nutrient limitation on land carbon sink projections.

To conclude, this study evaluates the impact of climate forcing biases and the nitrogen cycle on land carbon balance projections. Opportunities for future model development outlined above will allow us to explore the relative importance of additional processes and thereby advance our understanding of the terrestrial carbon cycle. Such efforts will yield more reliable carbon cycle projections and support the implementation of climate change policies designed to stabilize the climate system.

5 Tables

Table 1. Spinup duration, transient period, and future period for different forcing data sets.

Forcing data	Spinup N cycle off	 N cycle on	Transient	Future
CRUJRAv2	500 years	2300 years	1901-2014	NA
GSWP3-W5E	500 years	2300 years	1901-2014	NA
CanESM5	500 years	2300 years	1850-2014	2015-2099
Bias-adjusted CanESM5 (ISIMIP3b)	500 years	2300 years	1850-2014	2015-2099

Table 2. Simulations, meteorological forcing data, time period, and model configuration

Simulation ID	Forcing	Period	Nitrogen Cycle	Transient [CO_2]
CRUJRAv2	CRUJRAv2	historical	off	true
GSWP3-W5E5	GSWP3-W5E5	historical	off	true
CanESM5-hist	CanESM5	historical	off	true
CanESM5-ISIMIP3b-hist	bias-adjusted CanESM5 (ISIMIP3b)	historical	off	true
CanESM5-CRUJRAv2.RSDS-hist	CanESM5 with CRUJRAv2 RSDS	historical	off	true
CanESM5-CRUJRAv2.RLDS-hist	CanESM5 with CRUJRAv2 RLDS	historical	off	true
CanESM5-CRUJRAv2.TAS-hist	CanESM5 with CRUJRAv2 TAS	historical	off	true
CanESM5-CRUJRAv2.PRE-hist	CanESM5 with CRUJRAv2 PRE	historical	off	true
CanESM5-CRUJRAv2.HUSS-hist	CanESM5 with CRUJRAv2 HUSS	historical	off	true
CanESM5-CRUJRAv2.sfcWind-hist	CanESM5 with CRUJRAv2 WIND	historical	off	true
CanESM5-CRUJRAv2.PS-hist	CanESM5 with CRUJRAv2 PS	historical	off	true
CanESM5-SSP5-8.5	CanESM5	SSP5-8.5	off	true
CanESM5-ISIMIP3b-SSP5-8.5	bias-adjusted CanESM5 (ISIMIP3b)	SSP5-8.5	off	true
CRUJRAv2-NCycle	CRUJRAv2	historical	on	true
CanESM5-NCycle-hist	CanESM5	historical	on	true
CanESM5-NCycle-SSP5-8.5	CanESM5	SSP5-8.5	on	true
CanESM5-ISIMIP3b-NCycle-hist	bias-adjusted CanESM5 (ISIMIP3b)	historical	on	true
CanESM5-ISIMIP3b-NCycle-SSP5-8.5	bias-adjusted CanESM5 (ISIMIP3b)	SSP5-8.5	on	true
CRUJRAv2-NCycleV2	CRUJRAv2	historical	on	true
CanESM5-NCycleV2-hist	CanESM5	historical	on	true
CanESM5-NCycleV2-SSP5-8.5	CanESM5	SSP5-8.5	on	true
CanESM5-ISIMIP3b-NCycleV2-hist	bias-adjusted CanESM5 (ISIMIP3b)	historical	on	true
CanESM5-ISIMIP3b-NCycleV2-SSP5-8.5	bias-adjusted CanESM5 (ISIMIP3b)	SSP5-8.5	on	true
CRUJRAv2-CO2fixed	CRUJRAv2	historical	off	false
CanESM5-CO2fixed-hist	CanESM5	historical	off	false
CanESM5-CO2fixed-SSP5-8.5	CanESM5	SSP5-8.5	off	false

Table 3. Observation-based reference data used for model evaluation

Source	Variables	Approach	Period	Reference
AVHRR	LAI	artificial neural network	1982-2010	Claverie et al. (2016)
CAMS	NBP	atmospheric inversion	1979-2019	Agustí-Panareda et al. (2019)
CarboScope	NBP	atmospheric inversion	1999-2019	Rödenbeck et al. (2018)
CERES	ALBS, RSS, RLS, RNS	radiative transfer model	2000-2012	Kato et al. (2013)
CLASSr	RNS, HFLS, HFSS, HFG	blended product	2003-2009	Hobeichi et al. (2019)
Copernicus	LAI	artificial neural network	1999-2019	Verger et al. (2014)
CT2019	NBP, FIRE	inversion model	2000-2017	Jacobson et al. (2020)
ECCC	SNW	blended product	1981-2017	Mudryk (2020)
ESA	MRSLL	land surface model	1979-2017	Liu et al. (2011)
ESACCI	BURNT	burned-area mapping	2001-2017	Chuvieco et al. (2018)
FluxCom	GPP	machine learning	1980-2013	Jung et al. (2020)
FluxCom	RNS, HFLS, HFSS	machine learning	2001-2013	Jung et al. (2019)
GEWEXSRB	ALBS, RSS, RLS, RNS	radiative transfer model	1984-2007	Stackhouse et al. (2011)
GEOCARBON	AGB	machine learning	NA	Avitabile et al. (2016), Santoro et al. (2015)
GFED4S	BURNT	burned-area mapping	2001-2015	Giglio et al. (2010)
GOSIF	GPP	statistical model	2000-2017	X. Li and Xiao (2019)
HWSD	CSOIL	soil inventory	NA	Wieder (2014) Todd-Brown et al. (2013)
MODIS	ALBS	bidirectional reflectance distribution function	2000-2014	Strahler et al. (1999)
	LAI	radiative transfer model	2000-2017	Myneni et al. (2002)
SG250m	CSOIL	machine learning	NA	Hengl et al. (2017)
Zhang	AGB	data fusion	2000s	Zhang and Liang (2020)

623 ## 6 Figures

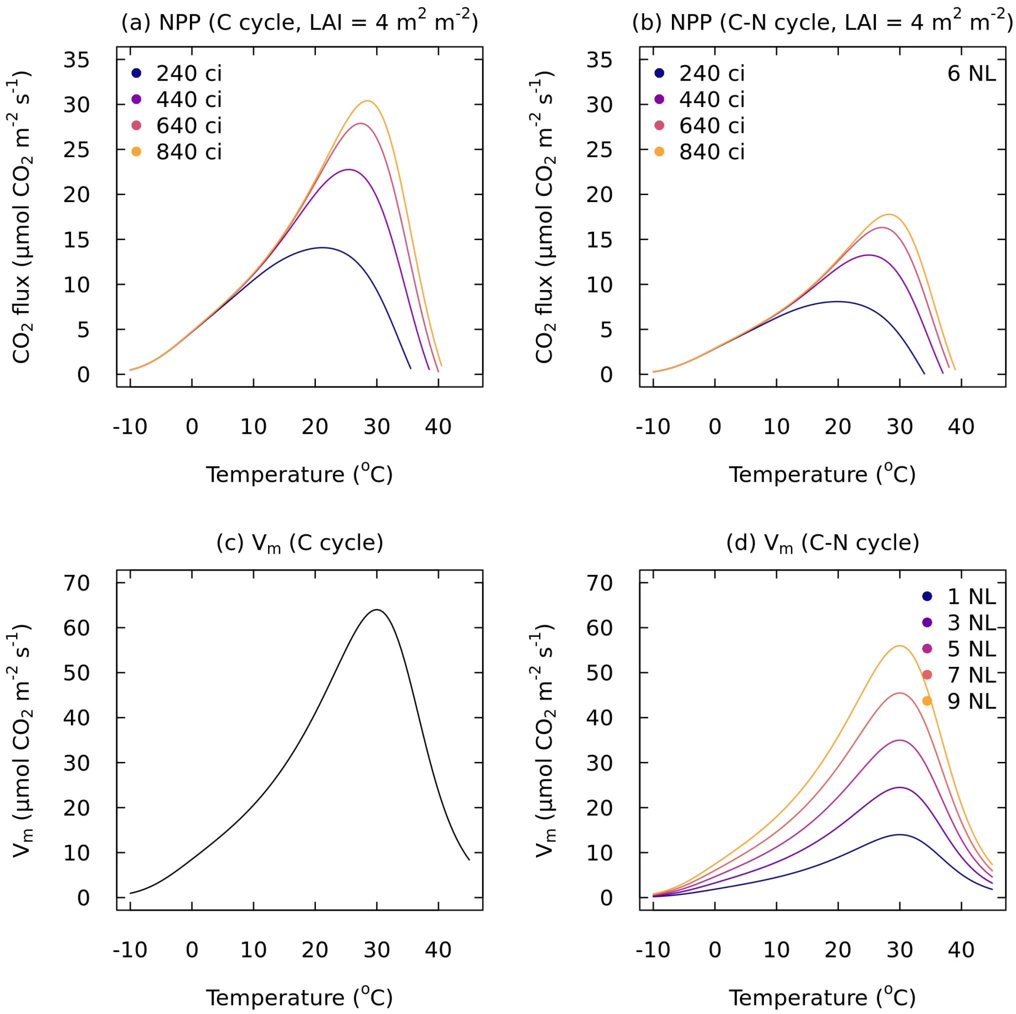

Figure 1. The model's sensitivity of (a, b) NPP and (c, d) maximum carboxylation rate to temperature when carbon-nitrogen coupling is (a, c) disabled and (b, d) enabled, where c_i is the partial pressure of CO_2 in the leaf interior in μmol mol^{-1} and N_L is the leaf nitrogen content in gN m^{-2} ground surface. The values are based on parameter values for a needleleaf evergreen PFT and constant values of carbon stocks and LAI representative for a location in the Canadian boreal forest.

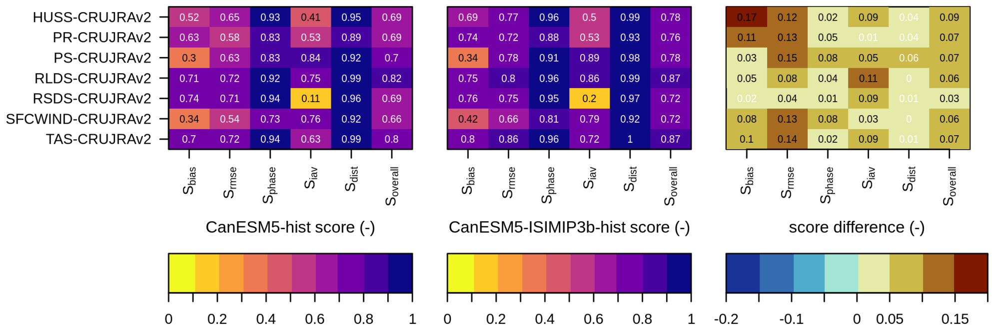

Figure 2. AMBER scores for meteorological forcing from raw CanESM5 data (CanESM5-hist) and bias-adjusted CanESM5 data (CanESM5-ISIMIP3b-hist) when evaluated against CRU-JRAv2, where HUSS is specific humidity, PR is precipitation, PS is surface pressure, RLDS is downwelling LW radiation, RSDS is downwelling SW radiation, SFCWIND is near-surface wind speed and TAS is near-surface air temperature. Score differences that are written in black font denote statistically significant differences at the 5% level (Wilcoxon test).

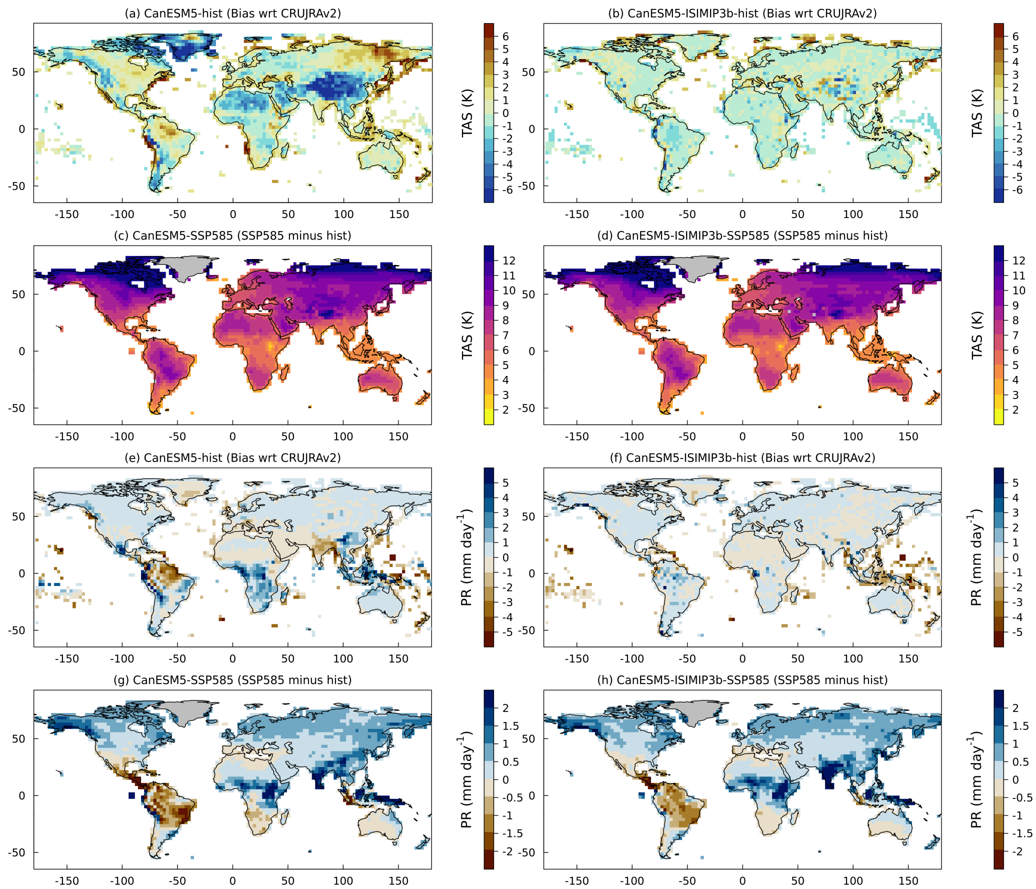

Figure 3. Annual mean near-surface temperature biases in (a) CanESM5-hist and (b) CanESM5-ISIMIP3b-hist (1995-2014), and future changes projected by (c) CanESM5-SSP5-8.5 and (d) CanESM5-ISIMIP3b-SSP5-8.5 (2080-2099 minus 1995-2014), as well as annual mean precipitation biases in (e) CanESM5-hist and (f) CanESM5-ISIMIP3b-hist, and future changes projected by (g) CanESM5-SSP5-8.5 and (h) CanESM5-ISIMIP3b-SSP5-8.5 (2080-2099 minus 1995-2014). The presence of fractional land cover in the CanESM5 land-sea mask explains the occurrence of grid cells in locations dominated by the ocean.

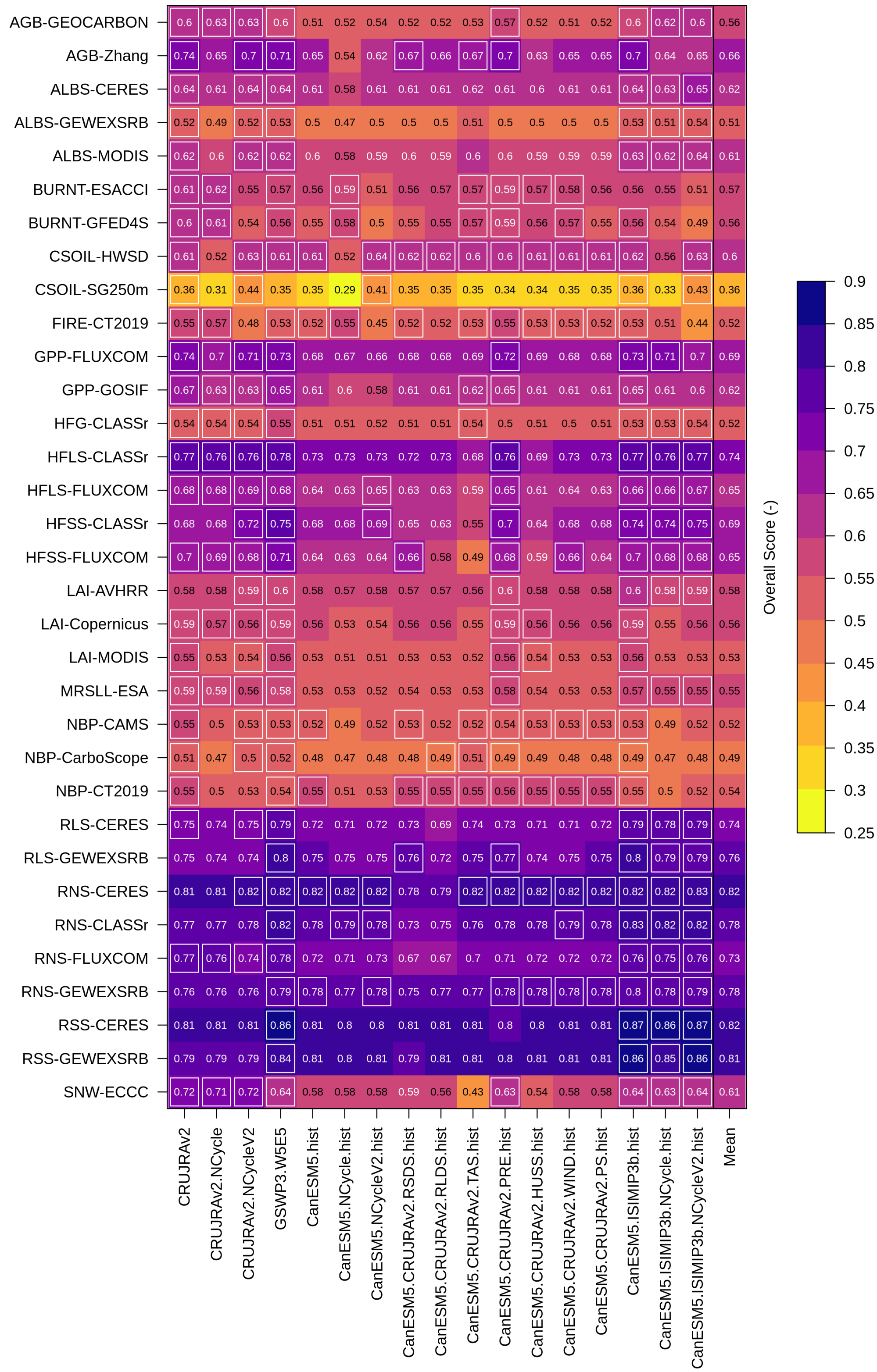

Figure 4. Model scores for each simulation, where higher scores imply better agreement with reference data (see section 2.5). White frames indicate values that exceed the corresponding multi-model mean values.

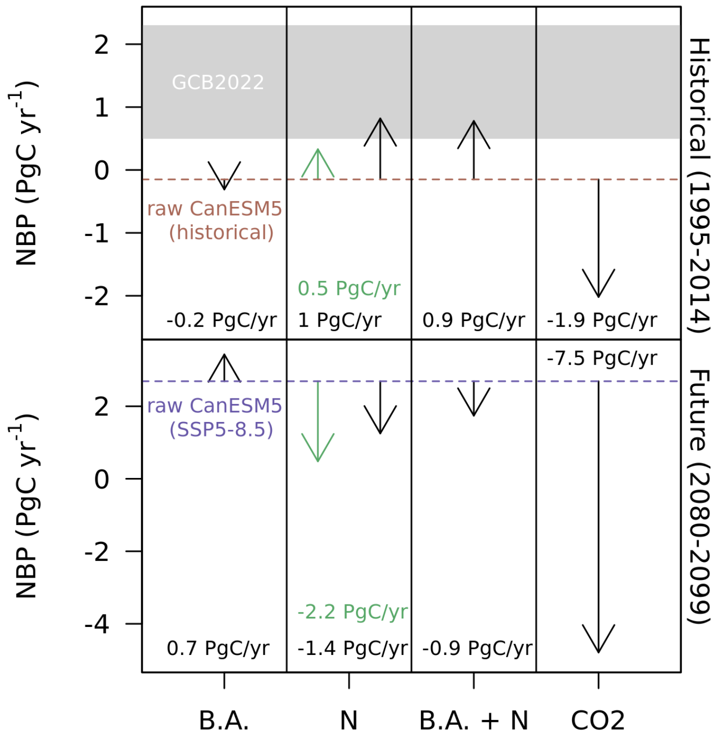

Figure 5. Impact of bias adjustment (B.A.), nitrogen cycle (N) parameter values, bias adjustment and nitrogen cycle combined (B.A. + N) and fixed [CO_2] on annual mean NBP. The stippled lines correspond to the NBP obtained when forcing CLASSIC with raw CanESM5 data. The grey swath provides the Global Carbon Budget 2022 uncertainty range for the years 2000-2009 (Friedlingstein et al., 2022). The numbers and arrows show the impact of a factor compared to the baseline simulation with raw CanESM5 data and no nitrogen cycle. Green arrows and green numbers correspond to the default nitrogen cycle parameter values.

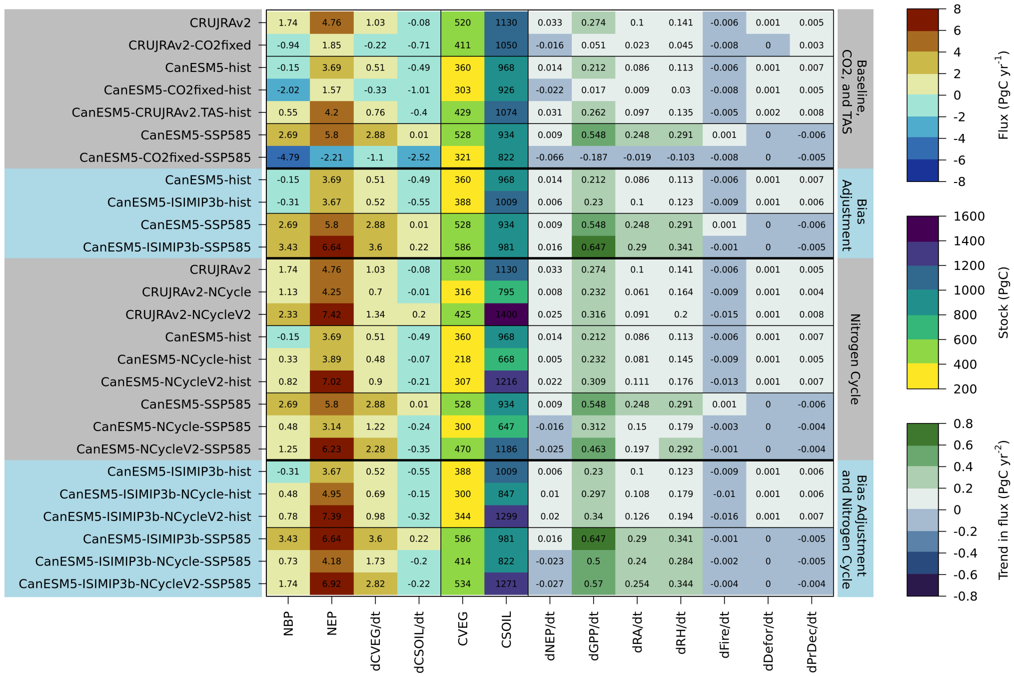

Figure 6. Global annual mean net biome productivity (NBP), net ecosystem productivity (NEP), vegetation carbon (CVEG) and soil organic carbon (CSOIL) of the last 20 years of simulations (1995-2014 for historical and 2080-2099 for SSP5-8.5) and linear trends of vegetation carbon, soil organic carbon, NEP, gross primary productivity (GPP), autotrophic respiration (RA), heterotrophic respiration (RH), and emissions from fires (Fire), deforestation (Defor), and decomposition of wood products (PrDec) of the last 50 years of simulations (1965-2014 for historical and 2050-2099 for SSP5-8.5) for a selection of experiments. Some simulations are listed multiple times to facilitate visual comparison. Values for all simulations are provided in Table S2-5.

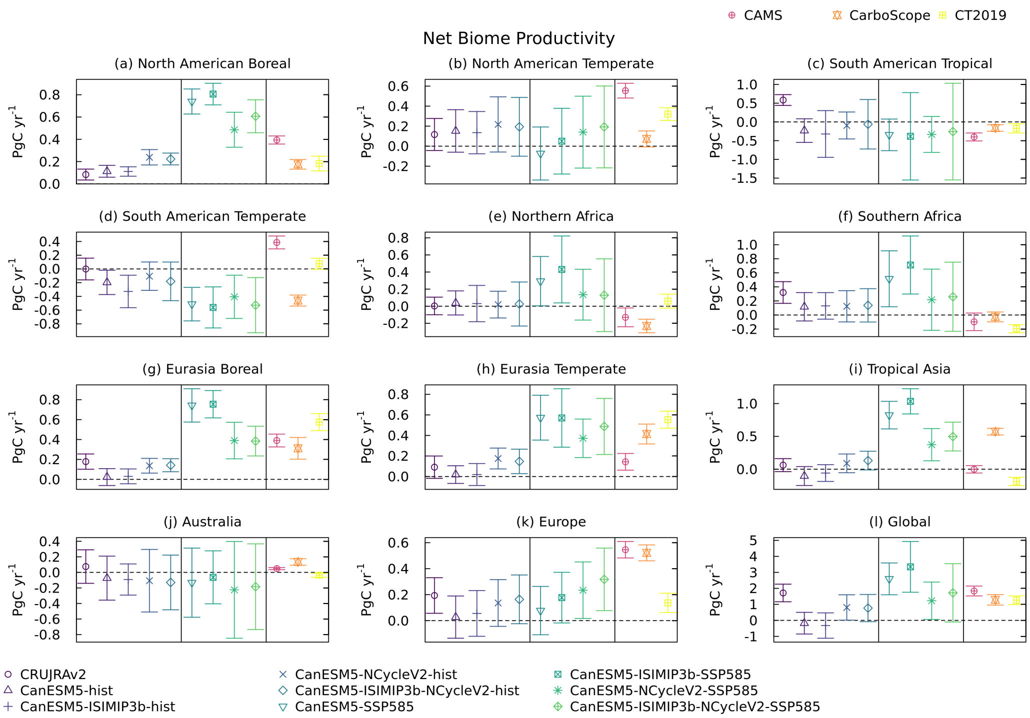

Figure 7. Annual net biome productivity and corresponding 95% confidence interval in different ecoregions during the historical (1995-2014) and future period under SSP5-8.5 (2080-2099). The periods of the reference data are listed in Table 3.

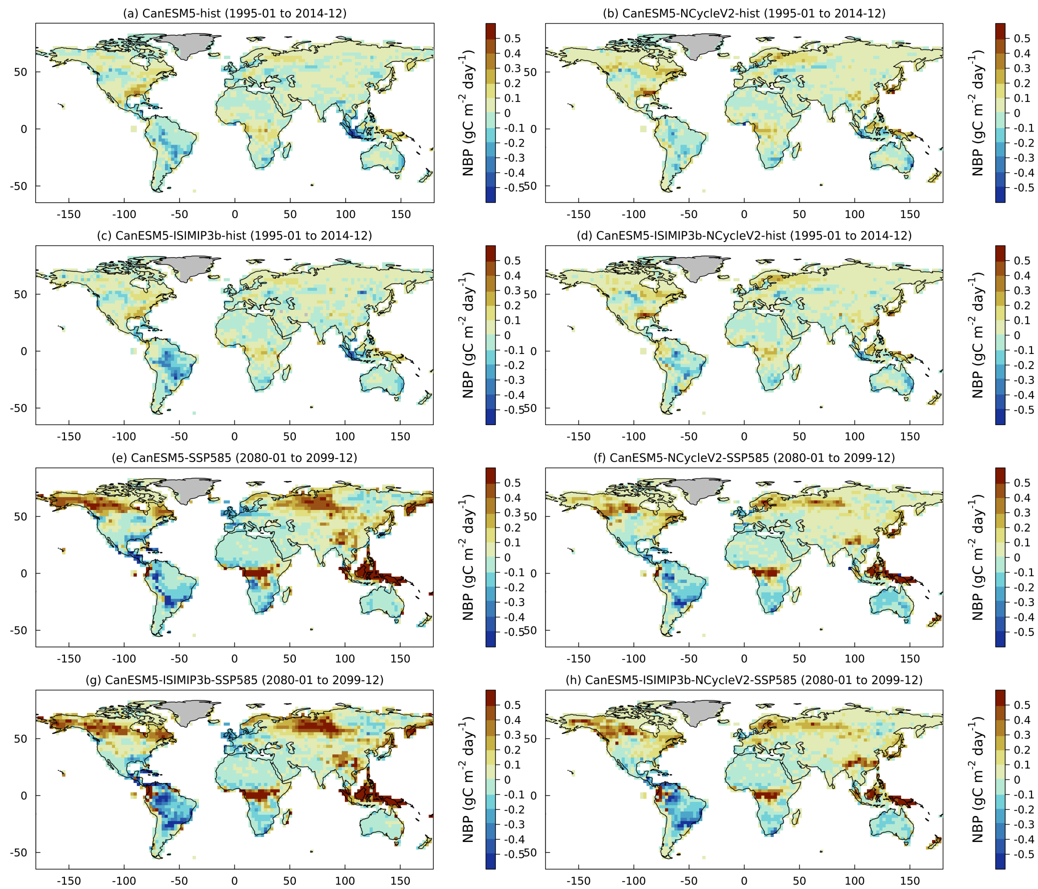

Figure 8. (a-d) Annual mean net biome productivity during the historical period (1995-2014) and (e-h) the corresponding projected changes (2080-2099) for a selection of simulations.

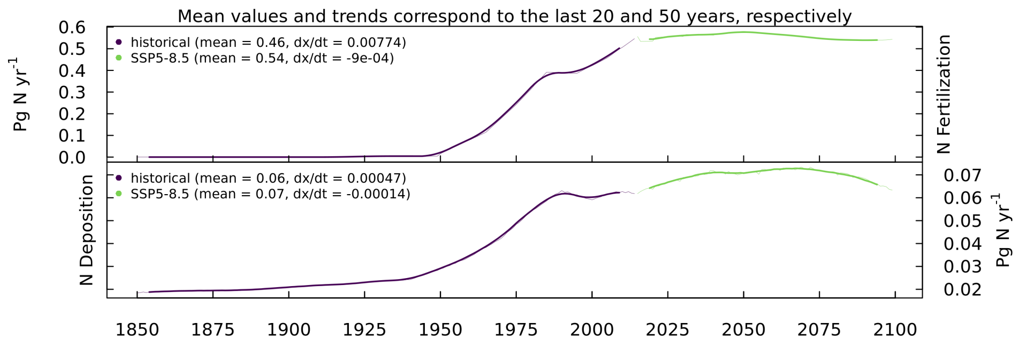

Figure 9. Prescribed nitrogen fertilization and deposition provided by the Coupled Model Intercomparison Project Phase 6.

Acknowledgments

The authors wish to thank Dr. Ed Chan for his assistance in processing CLASSIC input data. The authors express their appreciation to all groups who have made their reference data listed in Table 3 publicly available.

Open Research

The AMBER code, analysis scripts, analysis outputs, and the observation-based reference data used for model evaluation in this study can be downloaded from `https://doi.org/10.5281/zenodo.7799563`. The CLASSIC code is available at `https://doi.org/10.5281/zenodo.3522407`. The CLASSIC input data can be downloaded from (i) `https://crudata.uea.ac.uk/cru/data/hrg/` (CRUJRAv2), (ii) `https://esgf.llnl.gov/` (CanESM5), and (iii) `https://data.isimip.org` (bias-adjusted CanESM5 and GSWP3-W5E5).

References

Agustí-Panareda, A., Diamantakis, M., Massart, S., Chevallier, F., Muñoz-Sabater, J., Barré, J., ... Wunch, D. (2019, June). Modelling CO_2 weather – why horizontal resolution matters. *Atmos. Chem. Phys.*, *19*(11), 7347–7376.

Ahlström, A., Schurgers, G., & Smith, B. (2017, January). The large influence of climate model bias on terrestrial carbon cycle simulations. *Environ. Res. Lett.*, *12*(1), 014004.

Arora, V. K., & Boer, G. J. (2003, June). A representation of variable root distribution in dynamic vegetation models. *Earth Interact.*, *7*(6), 1–19.

Arora, V. K., & Boer, G. J. (2005a). Fire as an interactive component of dynamic vegetation models. *Journal of Geophysical Research: Biogeosciences*, *110*(G2).

Arora, V. K., & Boer, G. J. (2005b). A parameterization of leaf phenology for the terrestrial ecosystem component of climate models. *Glob. Chang. Biol.*.

Arora, V. K., & Boer, G. J. (2010). Uncertainties in the 20th century carbon budget associated with land use change. *Glob. Chang. Biol.*, *16*(12), 3327–3348.

Arora, V. K., Katavouta, A., Williams, R. G., Jones, C. D., Brovkin, V., Friedlingstein, P., ... Ziehn, T. (2020, August). Carbon–concentration and carbon–climate feedbacks in CMIP6 models and their comparison to CMIP5 models. *Biogeosciences*, *17*(16), 4173–4222.

Arora, V. K., & Melton, J. R. (2018, April). Reduction in global area burned and wildfire emissions since 1930s enhances carbon uptake by land. *Nat. Commun.*, *9*(1), 1326.

Asaadi, A., & Arora, V. K. (2021, January). Implementation of nitrogen cycle in the CLASSIC land model. *Biogeosciences*, *18*(2), 669–706.

Avitabile, V., Herold, M., Heuvelink, G. B. M., & others. (2016). An integrated pan tropical biomass map using multiple reference datasets. *Glob. Chang. Biol.*.

Belshe, E. F., Schuur, E. A. G., & Bolker, B. M. (2013, October). Tundra ecosystems observed to be CO2 sources due to differential amplification of the carbon cycle. *Ecol. Lett.*, *16*(10), 1307–1315.

Canadell, J., Monteiro, P., Costa, M., Cotrim da Cunha, L., Cox, P., Eliseev, A., ... Zickfeld, K. (2021). Global Carbon and other Biogeochemical Cycles and Feedbacks. In Climate Change 2021: The Physical Science Basis. Contribution of Working Group I to the Sixth Assessment Report of the Intergovernmental Panel on Climate Change. *Cambridge University Press*, 673-816.

Chuvieco, E., Lizundia-Loiola, J., Pettinari, M. L., Ramo, R., Padilla, M., Tansey, K., ... Others (2018). Generation and analysis of a new global burned area product based on MODIS 250 m reflectance bands and thermal anomalies. *Earth System Science Data*, *10*(4), 2015–2031.

Claverie, M., Matthews, J. L., Vermote, E. F., & Justice, C. O. (2016, March). A 30+ year AVHRR LAI and FAPAR climate data record: Algorithm description and validation. *Remote Sensing*, *8*(3), 263.

Collatz, G. J., Ball, J. T., Grivet, C., & Berry, J. A. (1991, April). Physiological and environmental regulation of stomatal conductance, photosynthesis and transpiration: a model that includes a laminar boundary layer. *Agric. For. Meteorol.*, *54*(2), 107–136.

Collatz, G. J., Ribas-Carbo, M., & Berry, J. A. (1992). Coupled Photosynthesis-Stomatal conductance model for leaves of C4 plants. *Funct. Plant Biol.*, *19*(5), 519–538.

Collier, N., Hoffman, F. M., Lawrence, D. M., Keppel-Aleks, G., Koven, C. D., Riley, W. J., … Randerson, J. T. (2018). The international land model benchmarking (ilamb) system: design, theory, and implementation. *Journal of Advances in Modeling Earth Systems*, *10*(11), 2731–2754.

Cucchi, M., Weedon, G. P., Amici, A., Bellouin, N., Lange, S., Schmied, H. M., … Buontempo, C. (2020). WFDE5: bias adjusted ERA5 reanalysis data for impact studies. *Earth System Science Data Discussions*, 1–32.

Elser, J. J., Bracken, M. E. S., Cleland, E. E., Gruner, D. S., Harpole, W. S., Hillebrand, H., … Smith, J. E. (2007, December). Global analysis of nitrogen and phosphorus limitation of primary producers in freshwater, marine and terrestrial ecosystems. *Ecol. Lett.*, *10*(12), 1135–1142.

Eyring, V., Gillett, N., Achuta Rao, K., Barimalala, R., Barreiro Parrillo, M., Bellouin, N., … Sun, Y. (2021). Human Influence on the Climate System. In Climate Change 2021: The Physical Science Basis. Contribution of Working Group I to the Sixth Assessment Report of the Intergovernmental Panel on Climate Change. *Cambridge University Press*, 423-552.

Fan, X., Duan, Q., Shen, C., Wu, Y., & Xing, C. (2020, October). Global surface air temperatures in CMIP6: historical performance and future changes. *Environ. Res. Lett.*, *15*(10), 104056.

Farquhar, G. D., von Caemmerer, S., & Berry, J. A. (1980, June). A biochemical model of photosynthetic CO2 assimilation in leaves of C 3 species. *Planta*, *149*(1), 78–90.

Friedlingstein, P., O'Sullivan, M., Jones, M. W., Andrew, R. M., Gregor, L., Hauck, J., … Zheng, B. (2022, November). Global carbon budget 2022. *Earth Syst. Sci. Data*, *14*(11), 4811–4900.

Giglio, L., Randerson, J., Van der Werf, G., Kasibhatla, P., Collatz, G., Morton, D., & DeFries, R. (2010). Assessing variability and long-term trends in burned area by merging multiple satellite fire products. *Biogeosciences*, *7*(3), 1171–1186.

Goll, D. S., Brovkin, V., Parida, B. R., Reick, C. H., Kattge, J., Reich, P. B., … Niinemets, Ü. (2012). Nutrient limitation reduces land carbon uptake in simulations with a model of combined carbon, nitrogen and phosphorus cycling. *Biogeosciences*, *9*, 3547–3569.

Guldberg, A., Kaas, E., Déqué, M., Yang, S., & Vester Thorsen, S. (2005, January). Reduction of systematic errors by empirical model correction: impact on seasonal prediction skill. *Tellus Ser. A Dyn. Meteorol. Oceanogr.*, *57*(4), 575–588.

Harris, I., Jones, P. D., Osborn, T. J., & others. (2014). Updated high-resolution grids of monthly climatic observations–the CRU TS3. 10 dataset. *International journal of climatology*, *34*(3), 623–642.

Hengl, T., de Jesus, J. M., Heuvelink, G. B. M., Gonzalez, M. R., Kilibarda, M., Blagotić, A., … Kempen, B. (2017). SoilGrids250m: Global gridded soil information based on machine learning. *PLoS One*, *12*(2), e0169748.

Hobeichi, S., Abramowitz, G., & Evans, J. (2019). Conserving land-atmosphere synthesis suite (CLASS). *J. Clim.*(2019).

Hopmans, J. W., & Bristow, K. L. (2002, January). Current capabilities and future needs of root water and nutrient uptake modeling. In D. L. Sparks (Ed.), *Advances in agronomy* (Vol. 77, pp. 103–183). Academic Press.

Huntzinger, D. N., Michalak, A. M., Schwalm, C., Ciais, P., King, A. W., Fang, Y., … Zhao, F. (2017, July). Uncertainty in the response of terrestrial carbon sink to environmental drivers undermines carbon-climate feedback predictions. *Sci. Rep.*, *7*(1), 4765.

Jacobson, A. R., Schuldt, K. N., Miller, J. B., Oda, T., Tans, P., Arlyn Andrews, … Miroslaw Zimnoch (2020). *Carbontracker ct2019.* NOAA Earth System Research Laboratory, Global Monitoring Division. Retrieved from `https://www.esrl.noaa.gov/gmd/ccgg/carbontracker/CT2019/` doi: 10.25925/39M3-6069

Jung, M., Koirala, S., Weber, U., Ichii, K., Gans, F., Camps-Valls, G., … Reichstein, M. (2019, May). The FLUXCOM ensemble of global land-atmosphere energy fluxes. *Sci Data*, *6*(1), 74.

Jung, M., Schwalm, C., Migliavacca, M., Walther, S., Camps-Valls, G., Koirala, S., … others (2020). Scaling carbon fluxes from eddy covariance sites to globe: synthesis and evaluation of the fluxcom approach. *Biogeosciences*, *17*(5), 1343–1365.

Kato, S., Loeb, N. G., Rose, F. G., Doelling, D. R., Rutan, D. A., Caldwell, T. E., … Weller, R. A. (2013, May). Surface irradiances consistent with CERES-Derived Top-of-Atmosphere shortwave and longwave irradiances. *J. Clim.*, *26*(9), 2719–2740.

Kattge, J., Knorr, W., Raddatz, T., & Wirth, C. (2009, April). Quantifying photosynthetic capacity and its relationship to leaf nitrogen content for global-scale terrestrial biosphere models. *Glob. Chang. Biol.*, *15*(4), 976–991.

Kobayashi, S., Ota, Y., Harada, Y., Ebita, A., Moriya, M., Onoda, H., … Takahashi, K. (2015). The JRA-55 reanalysis: General specifications and basic characteristics. *Journal of the Meteorological Society of Japan*, *93*(1), 5–48.

Kou-Giesbrecht, S., & Arora, V. (2022a, December). Compensatory effects between CO2, nitrogen deposition, and temperature in terrestrial biosphere models without nitrogen compromise projections of the future terrestrial carbon sink. *ESS Open Archive*. doi: 10.22541/essoar.167169640.09413994/v1

Kou-Giesbrecht, S., & Arora, V. K. (2022b, June). Representing the dynamic response of vegetation to nitrogen limitation via biological nitrogen fixation in the CLASSIC land model. *Global Biogeochem. Cycles*, *36*(6).

Koven, C. D., Ringeval, B., Friedlingstein, P., Ciais, P., Cadule, P., Khvorostyanov, D., … Tarnocai, C. (2011, September). Permafrost carbon-climate feedbacks accelerate global warming. *Proc. Natl. Acad. Sci. U. S. A.*, *108*(36), 14769–14774.

Krinner, G., Kharin, V., Roehrig, R., Scinocca, J., & Codron, F. (2020, October). Historically-based run-time bias corrections substantially improve model projections of 100 years of future climate change. *Communications Earth & Environment*, *1*(1), 1–7.

Lange, S. (2019). Trend-preserving bias adjustment and statistical downscaling with ISIMIP3BASD (v1. 0). *Geoscientific Model Development*, *12*(7).

Li, F., Val Martin, M., Andreae, M. O., Arneth, A., Hantson, S., Kaiser, J. W., … Rabin, S. S. (2019, October). Historical (1700–2012) global multi-model estimates of the fire emissions from the fire modeling intercomparison project (FireMIP). *Atmos. Chem. Phys.*, *19*(19), 12545–12567.

Li, X., & Xiao, J. (2019, October). Mapping photosynthesis solely from Solar-Induced chlorophyll fluorescence: A global, Fine-Resolution dataset of gross primary production derived from OCO-2. *Remote Sensing*, *11*(21), 2563.

Liu, Y. Y., Parinussa, R., Dorigo, W. A., De Jeu, R. A., Wagner, W., Van Dijk, A., … Evans, J. (2011). Developing an improved soil moisture dataset by

blending passive and active microwave satellite-based retrievals. *Hydrology and Earth System Sciences*, *15*(2), 425–436.
Loehman, R. A. (2020, October). Drivers of wildfire carbon emissions. *Nat. Clim. Chang.*, *10*(12), 1070–1071.
McGuire, A. D., Christensen, T. R., Hayes, D., Heroult, A., Euskirchen, E., Yi, Y., . . . Williams, M. (2012, April). An assessment of the carbon balance of arctic tundra: comparisons among observations, process models, and atmospheric inversions. *Biogeosci. Discuss.*, *9*(4), 4543–4594.
McGuire, A. D., Lawrence, D. M., Koven, C., Clein, J. S., Burke, E., Chen, G., . . . Zhuang, Q. (2018, April). Dependence of the evolution of carbon dynamics in the northern permafrost region on the trajectory of climate change. *Proc. Natl. Acad. Sci. U. S. A.*, *115*(15), 3882–3887.
Melton, J. R., & Arora, V. K. (2016, January). Competition between plant functional types in the canadian terrestrial ecosystem model (CTEM) v. 2.0. *Geoscientific Model Development*, *9*(1), 323–361.
Melton, J. R., Arora, V. K., Wisernig-Cojoc, E., Seiler, C., Fortier, M., Chan, E., & Teckentrup, L. (2020). Classic v1.0: the open-source community successor to the canadian land surface scheme (class) and the canadian terrestrial ecosystem model (ctem) – part 1: Model framework and site-level performance. *Geoscientific Model Development*, *13*(6), 2825–2850. Retrieved from `https://gmd.copernicus.org/articles/13/2825/2020/` doi: 10.5194/gmd-13-2825-2020
Melton, J. R., Shrestha, R. K., & Arora, V. K. (2015, February). The influence of soils on heterotrophic respiration exerts a strong control on net ecosystem productivity in seasonally dry amazonian forests. *Biogeosciences*, *12*(4), 1151–1168.
Melton, J. R., Verseghy, D. L., Sospedra-Alfonso, R., & Gruber, S. (2019, October). Improving permafrost physics in the coupled canadian land surface scheme (v.3.6.2) and canadian terrestrial ecosystem model (v.2.1) (CLASS-CTEM). *Geosci. Model Dev.*, *12*(10), 4443–4467.
Meyer, G., Humphreys, E. R., Melton, J. R., Cannon, A. J., & Lafleur, P. M. (2021, June). Simulating shrubs and their energy and carbon dioxide fluxes in canada's low arctic with the canadian land surface scheme including biogeochemical cycles (CLASSIC). *Biogeosciences*, *18*(11), 3263–3283.
Meyerholt, J., Sickel, K., & Zaehle, S. (2020, July). Ensemble projections elucidate effects of uncertainty in terrestrial nitrogen limitation on future carbon uptake. *Glob. Chang. Biol.*, *26*(7), 3978–3996.
Mudryk, L. (2020). *Historical gridded snow water equivalent and snow cover fraction over canada from remote sensing and land surface models.* `http://climate-scenarios.canada.ca/?page=blended-snow-data`. (Accessed: 2020-5-7)
Myneni, R. B., Hoffman, S., Knyazikhin, Y., Privette, J. L., Glassy, J., Tian, Y., . . . Running, S. W. (2002, November). Global products of vegetation leaf area and fraction absorbed PAR from year one of MODIS data. *Remote Sens. Environ.*, *83*(1), 214–231.
Padrón, R. S., Gudmundsson, L., Liu, L., Humphrey, V., & Seneviratne, S. I. (2022, December). Drivers of intermodel uncertainty in land carbon sink projections. *Biogeosciences*, *19*(23), 5435–5448.
Reed, S. C., Yang, X., & Thornton, P. E. (2015, October). Incorporating phosphorus cycling into global modeling efforts: a worthwhile, tractable endeavor. *New Phytol.*, *208*(2), 324–329.
Rödenbeck, C., Zaehle, S., Keeling, R., & Heimann, M. (2018, April). How does the terrestrial carbon exchange respond to inter-annual climatic variations? a quantification based on atmospheric CO_2 data. *Biogeosciences*, *15*(8), 2481–2498.

Rogelj, J., Shindell, D., Jiang, K., Fifita, S., Forster, P., Ginzburg, V., ... Vilarino, M. (2018). Mitigation pathways compatible with 1.5°c in the context of sustainable development. [Book Section]. In *Global warming of 1.5°c. an ipcc special report on the impacts of global warming of 1.5°c above pre-industrial levels and related global greenhouse gas emission pathways, in the context of strengthening the global response to the threat of climate change, sustainable development, and efforts to eradicate poverty* (p. 93-174). Cambridge, United Kingdom and New York, NY, USA: Cambridge University Press. Retrieved from `https://doi.org/10.1017/9781009157940.004` doi: 10.1017/9781009157940.004

Santoro, M., Beaudoin, A., Beer, C., Cartus, O., Fransson, J. E. S., Hall, R. J., ... Wegmüller, U. (2015, October). Forest growing stock volume of the northern hemisphere: Spatially explicit estimates for 2010 derived from envisat ASAR. *Remote Sens. Environ.*, *168*, 316–334.

Schneider von Deimling, T., Grosse, G., Strauss, J., Schirrmeister, L., Morgenstern, A., Schaphoff, S., ... Boike, J. (2015, June). Observation-based modelling of permafrost carbon fluxes with accounting for deep carbon deposits and thermokarst activity. *Biogeosciences*, *12*(11), 3469–3488.

Schultz, M. G., Heil, A., Hoelzemann, J. J., Spessa, A., Thonicke, K., Goldammer, J. G., ... van Het Bolscher, M. (2008). Global wildland fire emissions from 1960 to 2000. *Global Biogeochemical Cycles*, *22*(2).

Schuur, E. A. G., Abbott, B. W., Commane, R., Ernakovich, J., Euskirchen, E., Hugelius, G., ... Turetsky, M. (2022, October). Permafrost and climate change: Carbon cycle feedbacks from the warming arctic. *Annu. Rev. Environ. Resour.*, *47*(1), 343–371.

Seiler, C., Melton, J. R., Arora, V. K., Sitch, S., Friedlingstein, P., Anthoni, P., ... others (2022). Are terrestrial biosphere models fit for simulating the global land carbon sink? *Journal of Advances in Modeling Earth Systems*, *14*(5), e2021MS002946.

Seiler, C., Melton, J. R., Arora, V. K., & Wang, L. (2021, May). CLASSIC v1.0: the open-source community successor to the canadian land surface scheme (CLASS) and the canadian terrestrial ecosystem model (CTEM) – part 2: Global benchmarking. *Geoscientific Model Development*, *14*(5), 2371–2417.

Stackhouse, P. W., Jr, Gupta, S. K., Cox, S. J., Zhang, T., Mikovitz, J. C., & Hinkelman, L. M. (2011). The NASA/GEWEX surface radiation budget release 3.0: 24.5-year dataset. *Gewex news*, *21*(1), 10–12.

Strahler, A. H., Muller, J., Lucht, W., Schaaf, C., & others. (1999). MODIS BRDF/albedo product: algorithm theoretical basis document version 5.0. *MODIS*.

Swart, N. C., Cole, J. N. S., Kharin, V. V., Lazare, M., Scinocca, J. F., Gillett, N. P., ... Winter, B. (2019, November). The canadian earth system model version 5 (CanESM5.0.3). *Geoscientific Model Development*, *12*(11), 4823–4873.

Todd-Brown, K. E., Randerson, J. T., Post, W. M., Hoffman, F. M., Tarnocai, C., Schuur, E. A., & Allison, S. D. (2013). Causes of variation in soil carbon simulations from cmip5 earth system models and comparison with observations. *Biogeosciences*, *10*(3), 1717–1736.

Turetsky, M. R., Abbott, B. W., Jones, M. C., Anthony, K. W., Olefeldt, D., Schuur, E. A. G., ... McGuire, A. D. (2020, February). Carbon release through abrupt permafrost thaw. *Nat. Geosci.*, *13*(2), 138–143.

Tyukavina, A., Potapov, P., Hansen, M. C., Pickens, A. H., Stehman, S. V., Turubanova, S., ... Harris, N. (2022). Global trends of forest loss due to fire from 2001 to 2019. *Frontiers in Remote Sensing*, *3*.

UNFCCC. (2015). Adoption of the paris agreement, 21st conference of the parties. *United Nations*, 1-27.

Veraverbeke, S., Rogers, B. M., Goulden, M. L., Jandt, R. R., Miller, C. E., Wiggins, E. B., & Randerson, J. T. (2017, June). Lightning as a major driver of recent large fire years in north american boreal forests. *Nat. Clim. Chang.*, *7*(7), 529–534.

Verger, A., Baret, F., & Weiss, M. (2014). Near real-time vegetation monitoring at global scale. *IEEE Journal of Selected Topics in*.

Vitousek, P. M., Porder, S., Houlton, B. Z., & Chadwick, O. A. (2010, January). Terrestrial phosphorus limitation: mechanisms, implications, and nitrogen-phosphorus interactions. *Ecol. Appl.*, *20*(1), 5–15.

Wieder, W. (2014). *Regridded harmonized world soil database v1.2.* ORNL Distributed Active Archive Center. Retrieved from `http://daac.ornl.gov/cgi-bin/dsviewer.pl?ds_id=1247` doi: 10.3334/ORNLDAAC/1247

Zaehle, S., Friedlingstein, P., & Friend, A. D. (2010, January). Terrestrial nitrogen feedbacks may accelerate future climate change. *Geophys. Res. Lett.*, *37*(1).

Zhang, Y., & Liang, S. (2020, August). Fusion of multiple gridded biomass datasets for generating a global forest aboveground biomass map. *Remote Sensing*, *12*(16), 2559.

Figure 1.

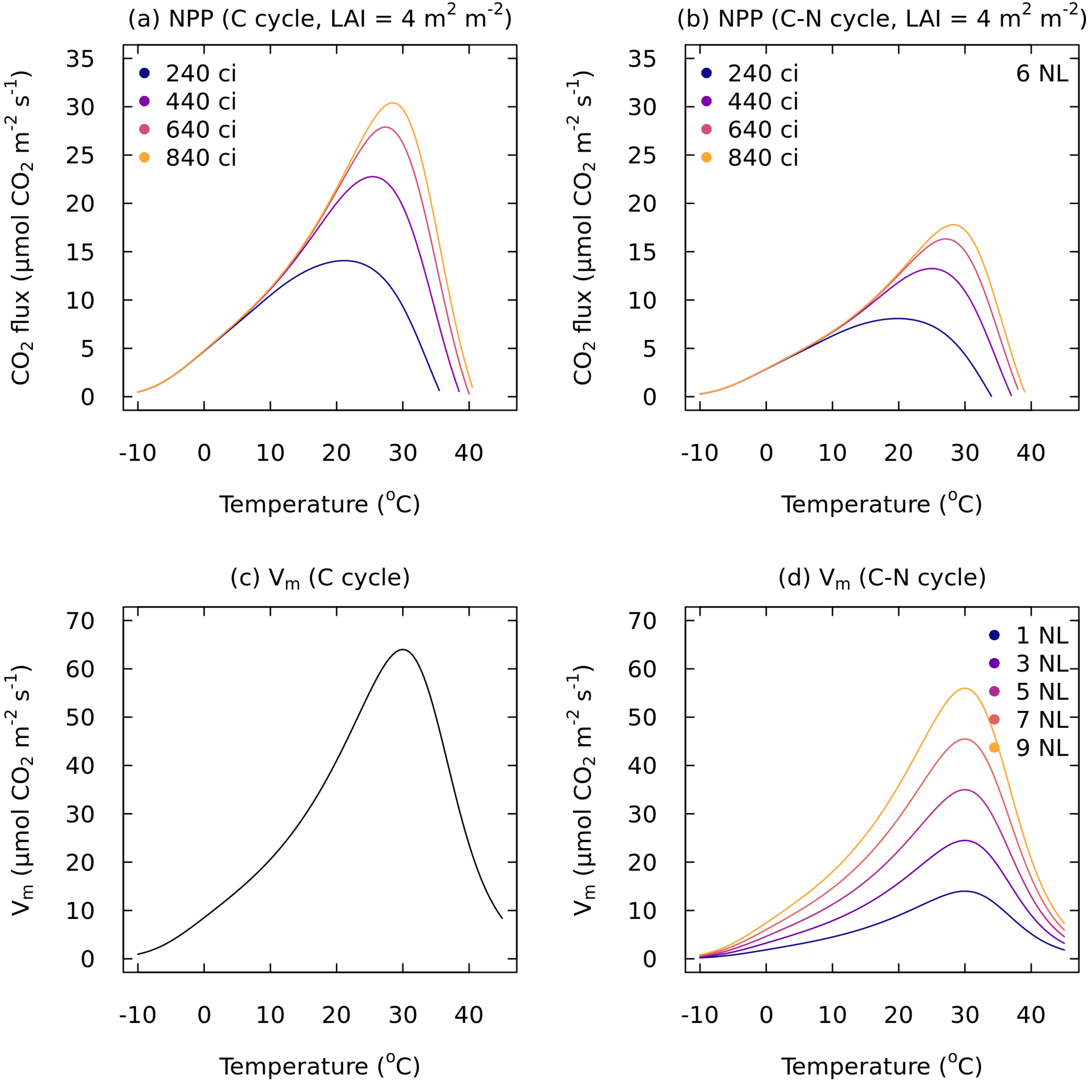
(a) NPP (C cycle, LAI = 4 m^2 m^{-2})
(b) NPP (C-N cycle, LAI = 4 m^2 m^{-2})
240 ci
440 ci
640 ci
840 ci
6 NL
CO_2 flux (μmol CO_2 m^{-2} s^{-1})
Temperature (^{o}C)
(c) V_m (C cycle)
(d) V_m (C-N cycle)
1 NL
3 NL
5 NL
7 NL
9 NL
V_m (μmol CO_2 m^{-2} s^{-1})
-10
0
10
20
30
40
35
25
15
5
70
60
50

Figure 2.

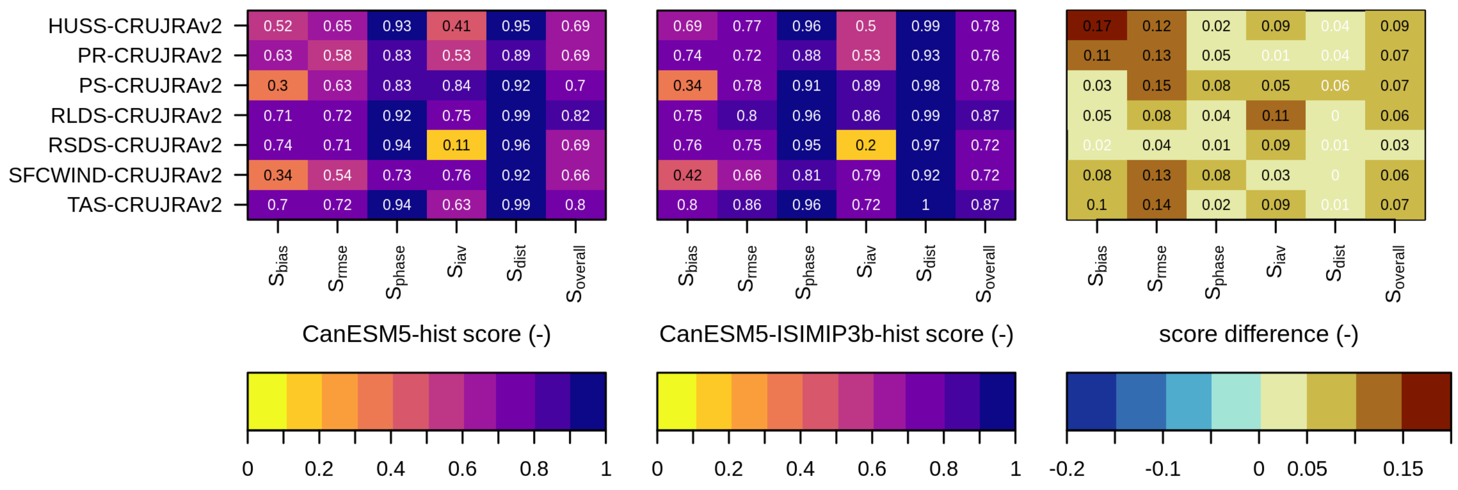

HUSS-CRUJRAv2
PR-CRUJRAv2
PS-CRUJRAv2
RLDS-CRUJRAv2
RSDS-CRUJRAv2
SFCWIND-CRUJRAv2
TAS-CRUJRAv2
S_{bias} S_{rmse} S_{phase} S_{iav} S_{dist} $S_{overall}$
CanESM5-hist score (-)
CanESM5-ISIMIP3b-hist score (-)
score difference (-)
0.52 0.65 0.93 0.41 0.95 0.69
0.63 0.58 0.83 0.53 0.89 0.69
0.3 0.63 0.83 0.84 0.92 0.7
0.71 0.72 0.92 0.75 0.99 0.82
0.74 0.71 0.94 0.11 0.96 0.69
0.34 0.54 0.73 0.76 0.92 0.66
0.7 0.72 0.94 0.63 0.99 0.8
0.69 0.77 0.96 0.5 0.99 0.78
0.74 0.72 0.88 0.53 0.93 0.76
0.34 0.78 0.91 0.89 0.98 0.78
0.75 0.8 0.96 0.86 0.99 0.87
0.76 0.75 0.95 0.2 0.97 0.72
0.42 0.66 0.81 0.79 0.92 0.72
0.8 0.86 0.96 0.72 1 0.87
0.17 0.12 0.02 0.09 0.04 0.09
0.11 0.13 0.05 0.01 0.04 0.07
0.03 0.15 0.08 0.05 0.06 0.07
0.05 0.08 0.04 0.11 0 0.06
0.02 0.04 0.01 0.09 0.01 0.03
0.08 0.13 0.08 0.03 0 0.06
0.1 0.14 0.02 0.09 0.01 0.07
0 0.2 0.4 0.6 0.8 1
0 0.2 0.4 0.6 0.8 1
-0.2 -0.1 0 0.05 0.15

Figure 3.

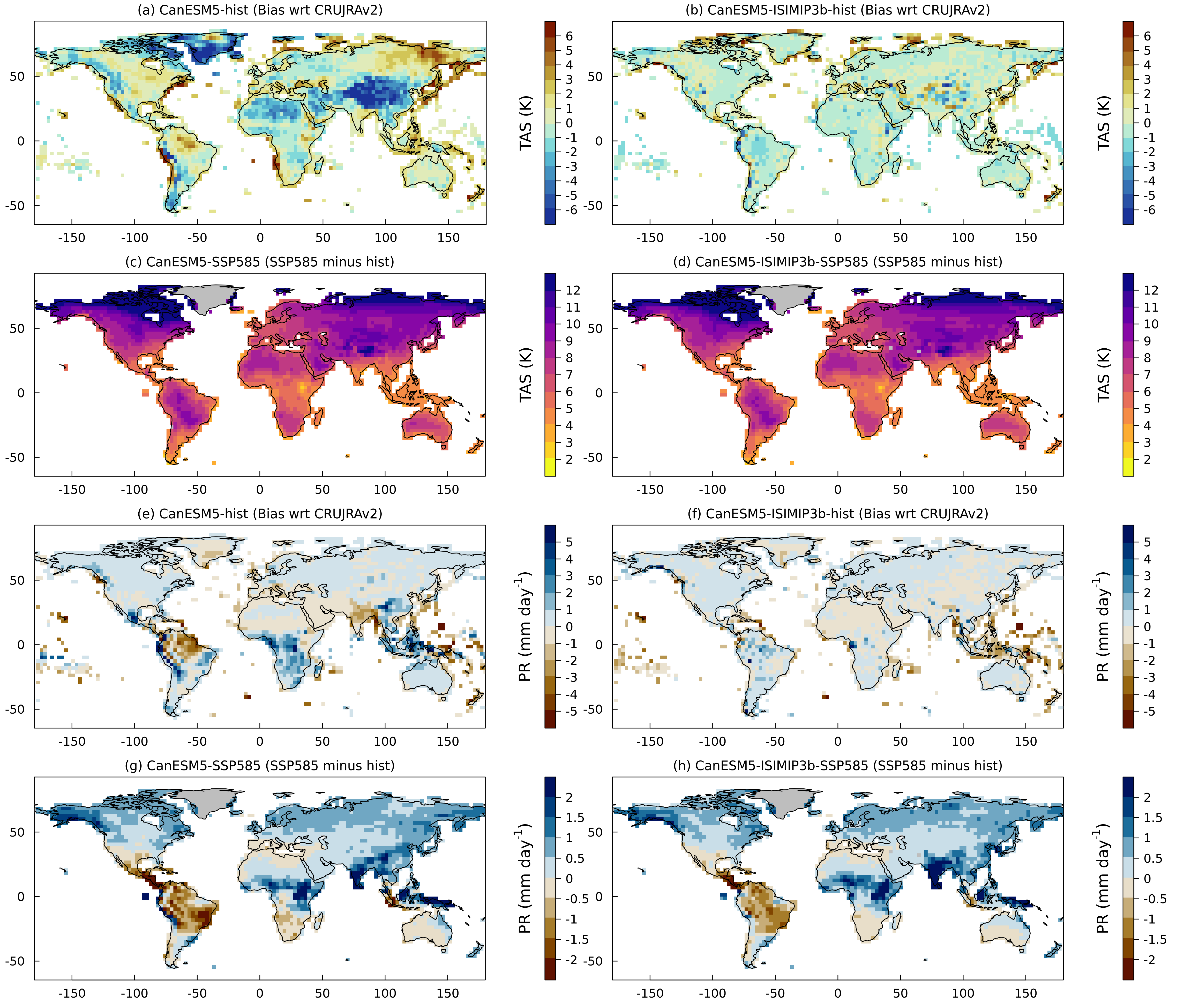
(a) CanESM5-hist (Bias wrt CRUJRAv2)
(b) CanESM5-ISIMIP3b-hist (Bias wrt CRUJRAv2)
TAS (K)
(c) CanESM5-SSP585 (SSP585 minus hist)
(d) CanESM5-ISIMIP3b-SSP585 (SSP585 minus hist)
TAS (K)
(e) CanESM5-hist (Bias wrt CRUJRAv2)
(f) CanESM5-ISIMIP3b-hist (Bias wrt CRUJRAv2)
PR (mm day-1)
(g) CanESM5-SSP585 (SSP585 minus hist)
(h) CanESM5-ISIMIP3b-SSP585 (SSP585 minus hist)
PR (mm day-1)

Figure 4.

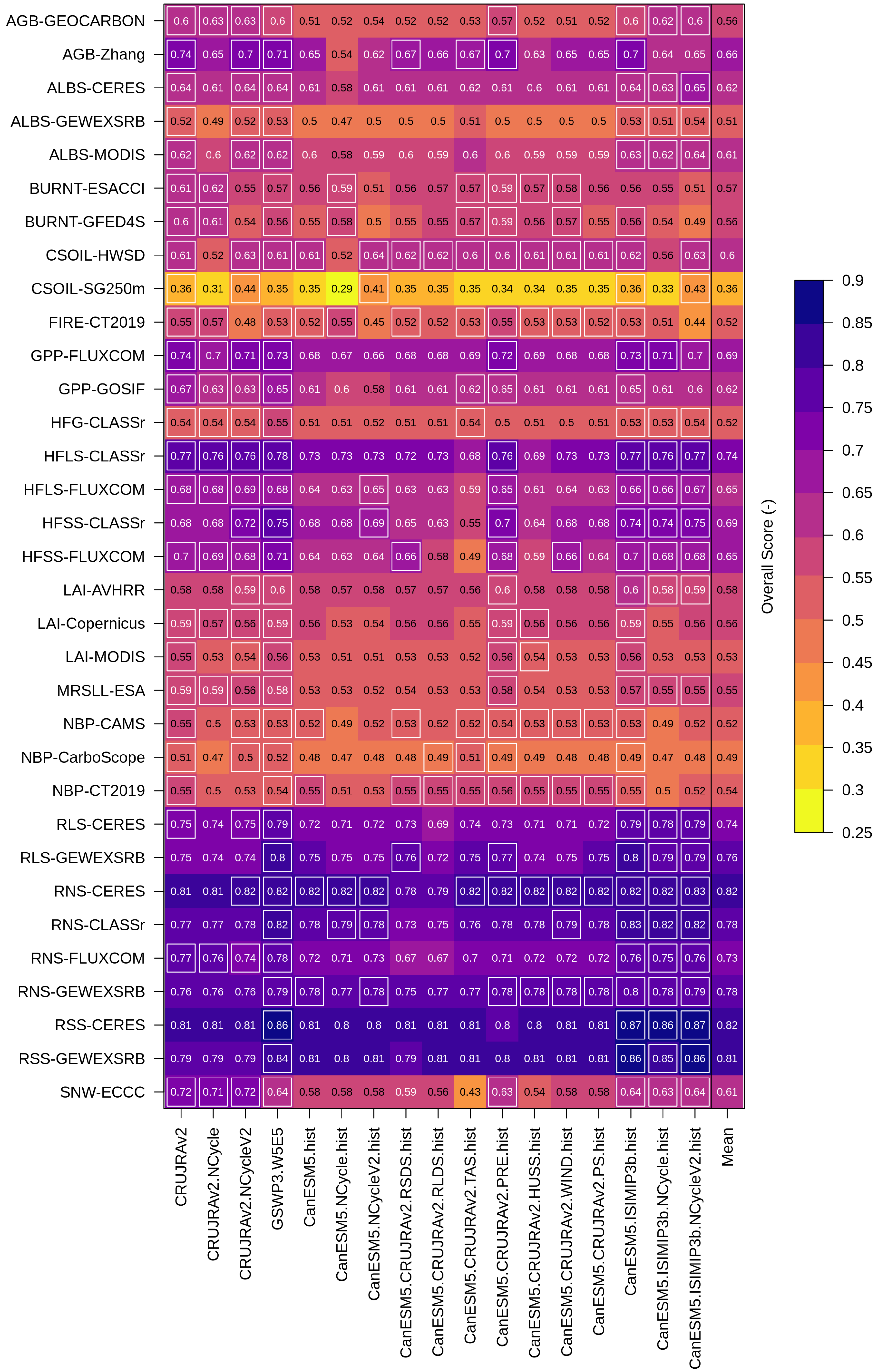

AGB-GEOCARBON 0.6 0.63 0.63 0.6 0.51 0.52 0.54 0.52 0.52 0.53 0.57 0.52 0.51 0.52 0.6 0.62 0.6 0.56
AGB-Zhang 0.74 0.65 0.7 0.71 0.65 0.54 0.62 0.67 0.66 0.67 0.7 0.63 0.65 0.65 0.7 0.64 0.65 0.66
ALBS-CERES 0.64 0.61 0.64 0.64 0.61 0.58 0.61 0.61 0.61 0.62 0.61 0.6 0.61 0.61 0.64 0.63 0.65 0.62
ALBS-GEWEXSRB 0.52 0.49 0.52 0.53 0.5 0.47 0.5 0.5 0.5 0.51 0.5 0.5 0.5 0.5 0.53 0.51 0.54 0.51
ALBS-MODIS 0.62 0.6 0.62 0.62 0.6 0.58 0.59 0.6 0.59 0.6 0.6 0.59 0.59 0.59 0.63 0.62 0.64 0.61
BURNT-ESACCI 0.61 0.62 0.55 0.57 0.56 0.59 0.51 0.56 0.57 0.57 0.59 0.57 0.58 0.56 0.56 0.55 0.51 0.57
BURNT-GFED4S 0.6 0.61 0.54 0.56 0.55 0.58 0.5 0.55 0.55 0.57 0.59 0.56 0.57 0.55 0.56 0.54 0.49 0.56
CSOIL-HWSD 0.61 0.52 0.63 0.61 0.61 0.52 0.64 0.62 0.62 0.6 0.6 0.61 0.61 0.61 0.62 0.56 0.63 0.6
CSOIL-SG250m 0.36 0.31 0.44 0.35 0.35 0.29 0.41 0.35 0.35 0.35 0.34 0.34 0.35 0.35 0.36 0.33 0.43 0.36
FIRE-CT2019 0.55 0.57 0.48 0.53 0.52 0.55 0.45 0.52 0.52 0.53 0.55 0.53 0.53 0.52 0.53 0.51 0.44 0.52
GPP-FLUXCOM 0.74 0.7 0.71 0.73 0.68 0.67 0.66 0.68 0.68 0.69 0.72 0.69 0.68 0.68 0.73 0.71 0.7 0.69
GPP-GOSIF 0.67 0.63 0.63 0.65 0.61 0.6 0.58 0.61 0.61 0.62 0.65 0.61 0.61 0.61 0.65 0.61 0.6 0.62
HFG-CLASSr 0.54 0.54 0.54 0.55 0.51 0.51 0.52 0.51 0.51 0.54 0.5 0.51 0.5 0.51 0.53 0.53 0.54 0.52
HFLS-CLASSr 0.77 0.76 0.76 0.78 0.73 0.73 0.73 0.72 0.73 0.68 0.76 0.69 0.73 0.73 0.77 0.76 0.77 0.74
HFLS-FLUXCOM 0.68 0.68 0.69 0.68 0.64 0.63 0.65 0.63 0.63 0.59 0.65 0.61 0.64 0.63 0.66 0.66 0.67 0.65
HFSS-CLASSr 0.68 0.68 0.72 0.75 0.68 0.68 0.69 0.65 0.63 0.55 0.7 0.64 0.68 0.68 0.74 0.74 0.75 0.69
HFSS-FLUXCOM 0.7 0.69 0.68 0.71 0.64 0.63 0.64 0.66 0.58 0.49 0.68 0.59 0.66 0.64 0.7 0.68 0.68 0.65
LAI-AVHRR 0.58 0.58 0.59 0.6 0.58 0.57 0.58 0.57 0.57 0.56 0.6 0.58 0.58 0.58 0.6 0.58 0.59 0.58
LAI-Copernicus 0.59 0.57 0.56 0.59 0.56 0.53 0.54 0.56 0.56 0.55 0.59 0.56 0.56 0.56 0.59 0.55 0.56 0.56
LAI-MODIS 0.55 0.53 0.54 0.56 0.53 0.51 0.51 0.53 0.53 0.52 0.56 0.54 0.53 0.53 0.56 0.53 0.53 0.53
MRSLL-ESA 0.59 0.59 0.56 0.58 0.53 0.53 0.52 0.54 0.53 0.53 0.58 0.54 0.53 0.53 0.57 0.55 0.55 0.55
NBP-CAMS 0.55 0.5 0.53 0.53 0.52 0.49 0.52 0.53 0.52 0.52 0.54 0.53 0.53 0.53 0.53 0.49 0.52 0.52
NBP-CarboScope 0.51 0.47 0.5 0.52 0.48 0.47 0.48 0.48 0.49 0.51 0.49 0.49 0.48 0.48 0.49 0.47 0.48 0.49
NBP-CT2019 0.55 0.5 0.53 0.54 0.55 0.51 0.53 0.55 0.55 0.55 0.56 0.55 0.55 0.55 0.55 0.5 0.52 0.54
RLS-CERES 0.75 0.74 0.75 0.79 0.72 0.71 0.72 0.73 0.69 0.74 0.73 0.71 0.71 0.72 0.79 0.78 0.79 0.74
RLS-GEWEXSRB 0.75 0.74 0.74 0.8 0.75 0.75 0.75 0.76 0.72 0.75 0.77 0.74 0.75 0.75 0.8 0.79 0.79 0.76
RNS-CERES 0.81 0.81 0.82 0.82 0.82 0.82 0.82 0.78 0.79 0.82 0.82 0.82 0.82 0.82 0.82 0.82 0.83 0.82
RNS-CLASSr 0.77 0.77 0.78 0.82 0.78 0.79 0.78 0.73 0.75 0.76 0.78 0.78 0.79 0.78 0.83 0.82 0.82 0.78
RNS-FLUXCOM 0.77 0.76 0.74 0.78 0.72 0.71 0.73 0.67 0.67 0.7 0.71 0.72 0.72 0.72 0.76 0.75 0.76 0.73
RNS-GEWEXSRB 0.76 0.76 0.76 0.79 0.78 0.77 0.78 0.75 0.77 0.77 0.78 0.78 0.78 0.78 0.8 0.78 0.79 0.78
RSS-CERES 0.81 0.81 0.81 0.86 0.81 0.8 0.8 0.81 0.81 0.81 0.8 0.8 0.81 0.81 0.87 0.86 0.87 0.82
RSS-GEWEXSRB 0.79 0.79 0.79 0.84 0.81 0.8 0.81 0.79 0.81 0.81 0.8 0.81 0.81 0.81 0.86 0.85 0.86 0.81
SNW-ECCC 0.72 0.71 0.72 0.64 0.58 0.58 0.58 0.59 0.56 0.43 0.63 0.54 0.58 0.58 0.64 0.63 0.64 0.61
CRUJRAv2
CRUJRAv2.NCycle
CRUJRAv2.NCycleV2
GSWP3.W5E5
CanESM5.hist
CanESM5.NCycle.hist
CanESM5.NCycleV2.hist
CanESM5.CRUJRAv2.RSDS.hist
CanESM5.CRUJRAv2.RLDS.hist
CanESM5.CRUJRAv2.TAS.hist
CanESM5.CRUJRAv2.PRE.hist
CanESM5.CRUJRAv2.HUSS.hist
CanESM5.CRUJRAv2.WIND.hist
CanESM5.CRUJRAv2.PS.hist
CanESM5.ISIMIP3b.hist
CanESM5.ISIMIP3b.NCycle.hist
CanESM5.ISIMIP3b.NCycleV2.hist
Mean
Overall Score (-)
0.9
0.85
0.8
0.75
0.7
0.65
0.6
0.55
0.5
0.45
0.4
0.35
0.3
0.25

Figure 5.

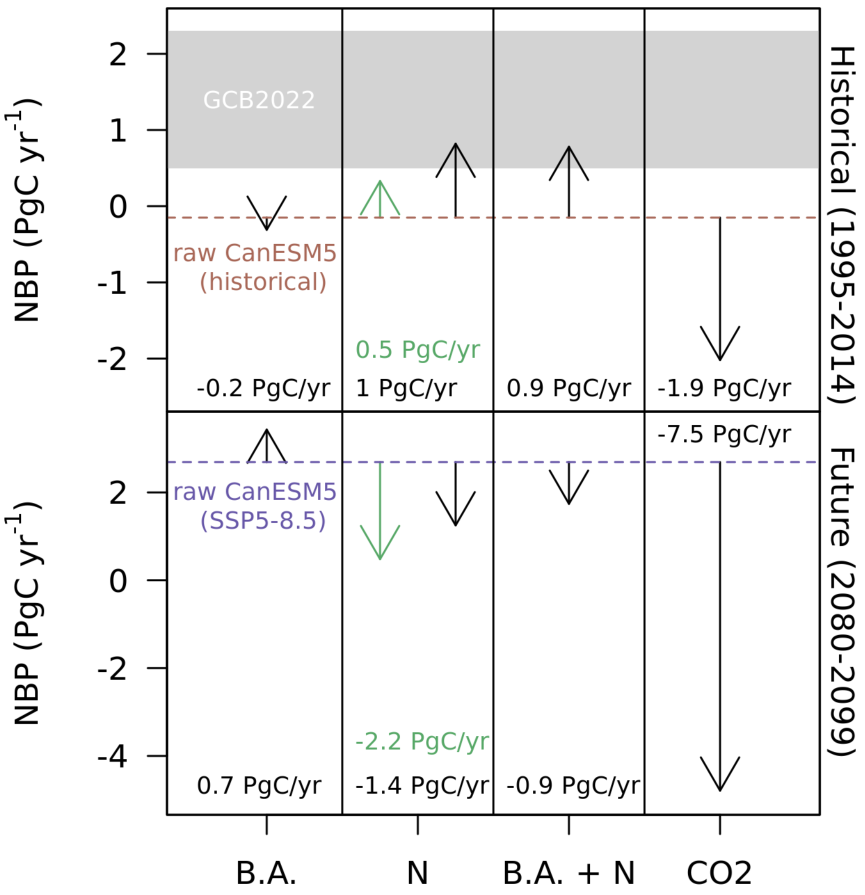

NBP (PgC yr^{-1})
2
1
0
-1
-2
GCB2022
raw CanESM5
(historical)
0.5 PgC/yr
-0.2 PgC/yr
1 PgC/yr
0.9 PgC/yr
-1.9 PgC/yr
Historical (1995-2014)
NBP (PgC yr^{-1})
2
0
-2
-4
-7.5 PgC/yr
raw CanESM5
(SSP5-8.5)
-2.2 PgC/yr
0.7 PgC/yr
-1.4 PgC/yr
-0.9 PgC/yr
Future (2080-2099)
B.A.
N
B.A. + N
CO2

Figure 6.

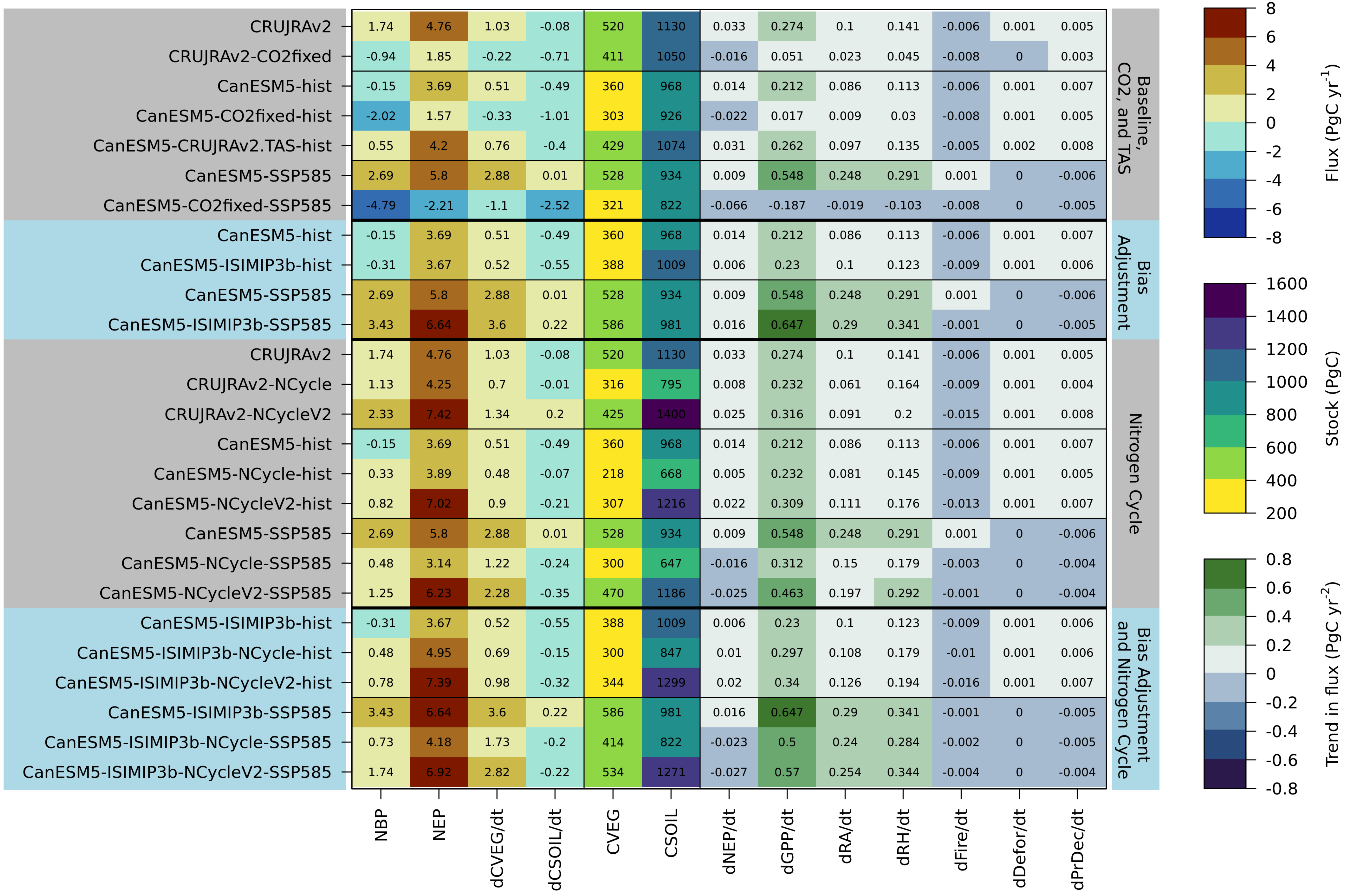

CRUJRAv2 1.74 4.76 1.03 -0.08 520 1130 0.033 0.274 0.1 0.141 -0.006 0.001 0.005
CRUJRAv2-CO2fixed -0.94 1.85 -0.22 -0.71 411 1050 -0.016 0.051 0.023 0.045 -0.008 0 0.003
CanESM5-hist -0.15 3.69 0.51 -0.49 360 968 0.014 0.212 0.086 0.113 -0.006 0.001 0.007
CanESM5-CO2fixed-hist -2.02 1.57 -0.33 -1.01 303 926 -0.022 0.017 0.009 0.03 -0.008 0.001 0.005
CanESM5-CRUJRAv2.TAS-hist 0.55 4.2 0.76 -0.4 429 1074 0.031 0.262 0.097 0.135 -0.005 0.002 0.008
CanESM5-SSP585 2.69 5.8 2.88 0.01 528 934 0.009 0.548 0.248 0.291 0.001 0 -0.006
CanESM5-CO2fixed-SSP585 -4.79 -2.21 -1.1 -2.52 321 822 -0.066 -0.187 -0.019 -0.103 -0.008 0 -0.005
CanESM5-hist -0.15 3.69 0.51 -0.49 360 968 0.014 0.212 0.086 0.113 -0.006 0.001 0.007
CanESM5-ISIMIP3b-hist -0.31 3.67 0.52 -0.55 388 1009 0.006 0.23 0.1 0.123 -0.009 0.001 0.006
CanESM5-SSP585 2.69 5.8 2.88 0.01 528 934 0.009 0.548 0.248 0.291 0.001 0 -0.006
CanESM5-ISIMIP3b-SSP585 3.43 6.64 3.6 0.22 586 981 0.016 0.647 0.29 0.341 -0.001 0 -0.005
CRUJRAv2 1.74 4.76 1.03 -0.08 520 1130 0.033 0.274 0.1 0.141 -0.006 0.001 0.005
CRUJRAv2-NCycle 1.13 4.25 0.7 -0.01 316 795 0.008 0.232 0.061 0.164 -0.009 0.001 0.004
CRUJRAv2-NCycleV2 2.33 7.42 1.34 0.2 425 1400 0.025 0.316 0.091 0.2 -0.015 0.001 0.008
CanESM5-hist -0.15 3.69 0.51 -0.49 360 968 0.014 0.212 0.086 0.113 -0.006 0.001 0.007
CanESM5-NCycle-hist 0.33 3.89 0.48 -0.07 218 668 0.005 0.232 0.081 0.145 -0.009 0.001 0.005
CanESM5-NCycleV2-hist 0.82 7.02 0.9 -0.21 307 1216 0.022 0.309 0.111 0.176 -0.013 0.001 0.007
CanESM5-SSP585 2.69 5.8 2.88 0.01 528 934 0.009 0.548 0.248 0.291 0.001 0 -0.006
CanESM5-NCycle-SSP585 0.48 3.14 1.22 -0.24 300 647 -0.016 0.312 0.15 0.179 -0.003 0 -0.004
CanESM5-NCycleV2-SSP585 1.25 6.23 2.28 -0.35 470 1186 -0.025 0.463 0.197 0.292 -0.001 0 -0.004
CanESM5-ISIMIP3b-hist -0.31 3.67 0.52 -0.55 388 1009 0.006 0.23 0.1 0.123 -0.009 0.001 0.006
CanESM5-ISIMIP3b-NCycle-hist 0.48 4.95 0.69 -0.15 300 847 0.01 0.297 0.108 0.179 -0.01 0.001 0.006
CanESM5-ISIMIP3b-NCycleV2-hist 0.78 7.39 0.98 -0.32 344 1299 0.02 0.34 0.126 0.194 -0.016 0.001 0.007
CanESM5-ISIMIP3b-SSP585 3.43 6.64 3.6 0.22 586 981 0.016 0.647 0.29 0.341 -0.001 0 -0.005
CanESM5-ISIMIP3b-NCycle-SSP585 0.73 4.18 1.73 -0.2 414 822 -0.023 0.5 0.24 0.284 -0.002 0 -0.005
CanESM5-ISIMIP3b-NCycleV2-SSP585 1.74 6.92 2.82 -0.22 534 1271 -0.027 0.57 0.254 0.344 -0.004 0 -0.004
NBP
NEP
dCVEG/dt
dCSOIL/dt
CVEG
CSOIL
dNEP/dt
dGPP/dt
dRA/dt
dRH/dt
dFire/dt
dDefor/dt
dPrDec/dt
Baseline, CO2, and TAS
Bias Adjustment
Nitrogen Cycle
Bias Adjustment and Nitrogen Cycle
Flux (PgC yr-1)
8 6 4 2 0 -2 -4 -6 -8
Stock (PgC)
1600 1400 1200 1000 800 600 400 200
Trend in flux (PgC yr-2)
0.8 0.6 0.4 0.2 0 -0.2 -0.4 -0.6 -0.8

Figure 7.

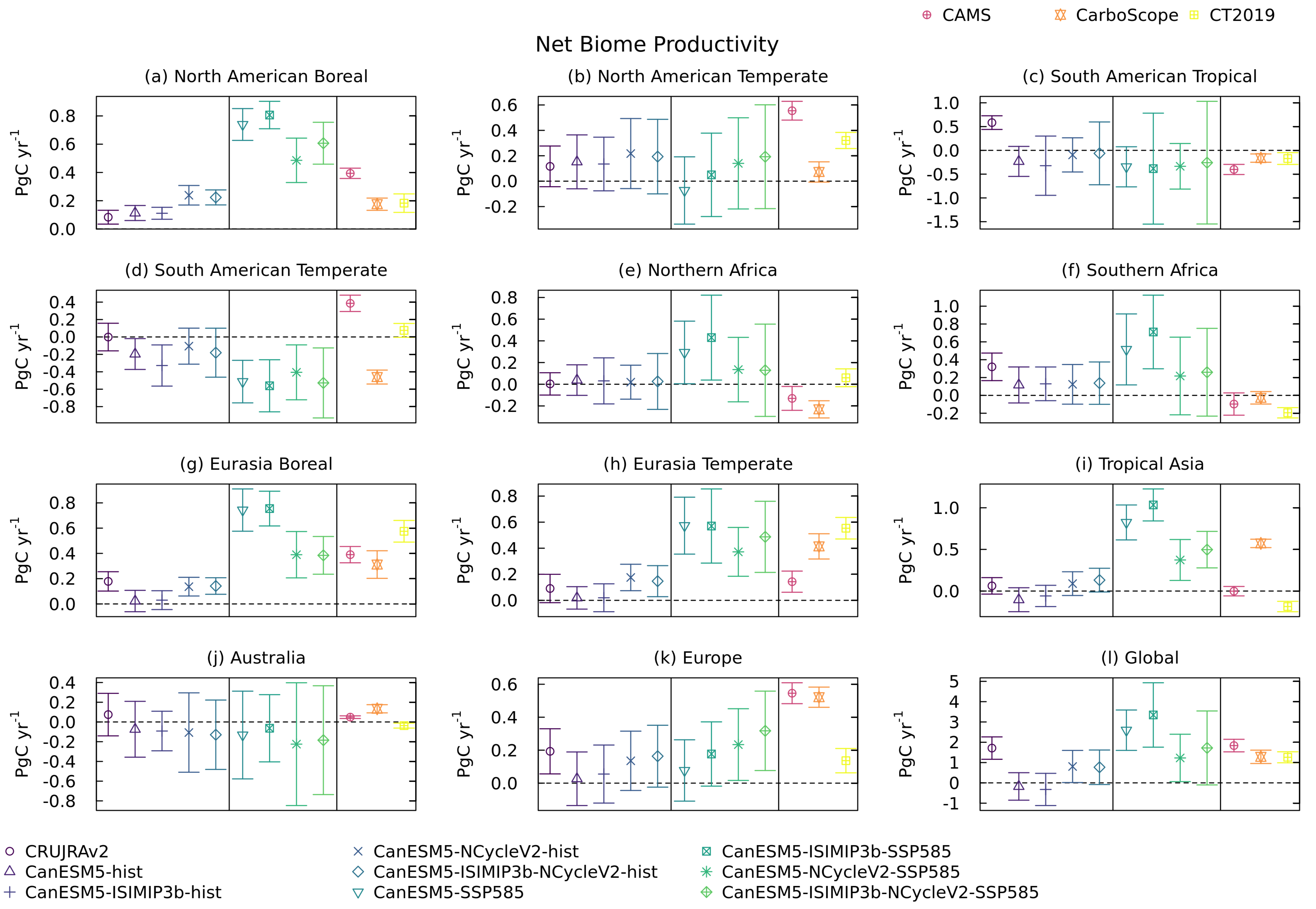
Net Biome Productivity
CAMS
CarboScope
CT2019
(a) North American Boreal
(b) North American Temperate
(c) South American Tropical
(d) South American Temperate
(e) Northern Africa
(f) Southern Africa
(g) Eurasia Boreal
(h) Eurasia Temperate
(i) Tropical Asia
(j) Australia
(k) Europe
(l) Global
PgC yr-1
CRUJRAv2
CanESM5-hist
CanESM5-ISIMIP3b-hist
CanESM5-NCycleV2-hist
CanESM5-ISIMIP3b-NCycleV2-hist
CanESM5-SSP585
CanESM5-ISIMIP3b-SSP585
CanESM5-NCycleV2-SSP585
CanESM5-ISIMIP3b-NCycleV2-SSP585

Figure 8.

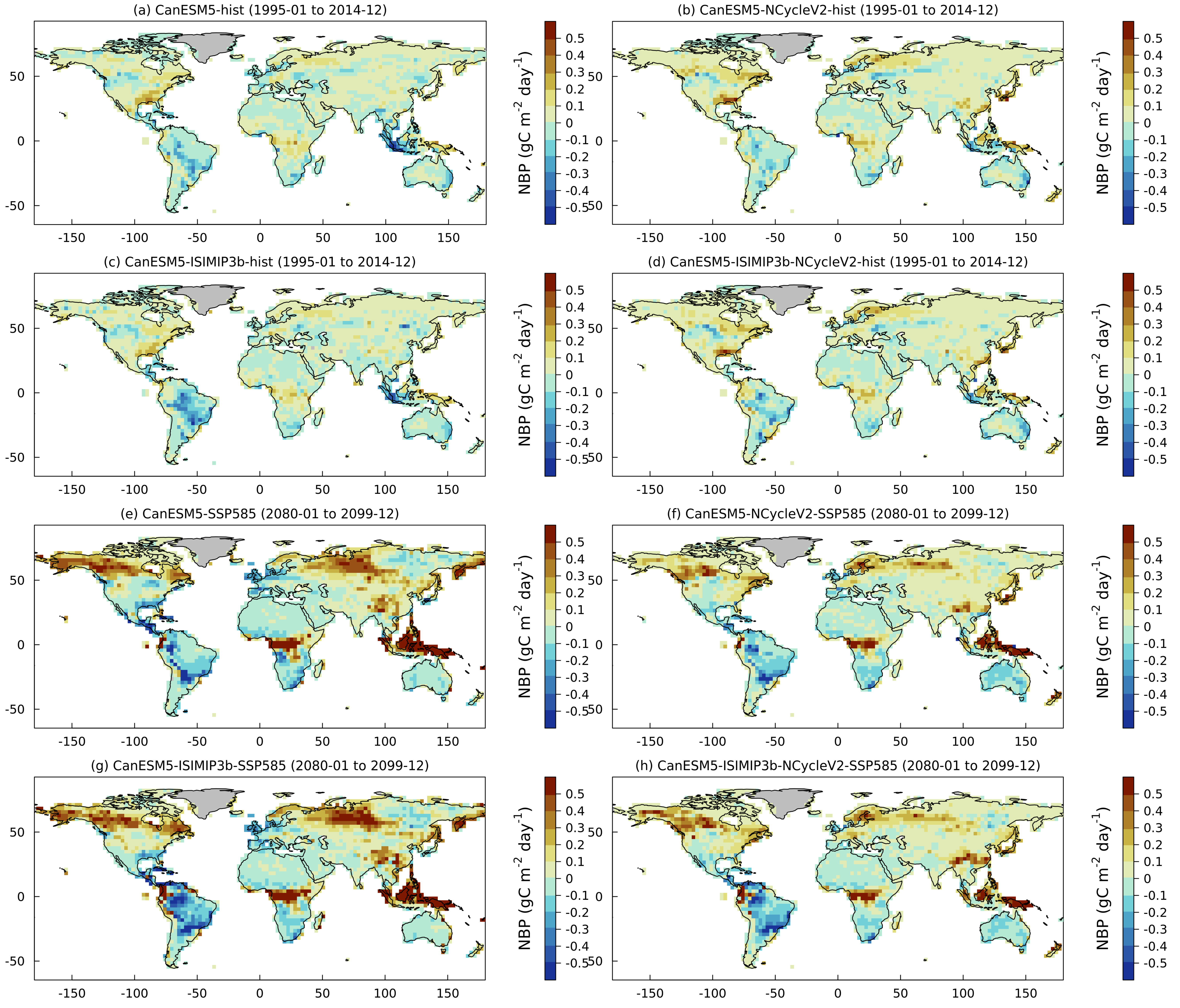
(a) CanESM5-hist (1995-01 to 2014-12)
(b) CanESM5-NCycleV2-hist (1995-01 to 2014-12)
(c) CanESM5-ISIMIP3b-hist (1995-01 to 2014-12)
(d) CanESM5-ISIMIP3b-NCycleV2-hist (1995-01 to 2014-12)
(e) CanESM5-SSP585 (2080-01 to 2099-12)
(f) CanESM5-NCycleV2-SSP585 (2080-01 to 2099-12)
(g) CanESM5-ISIMIP3b-SSP585 (2080-01 to 2099-12)
(h) CanESM5-ISIMIP3b-NCycleV2-SSP585 (2080-01 to 2099-12)
NBP (gC m^{-2} day^{-1})
0.5
0.4
0.3
0.2
0.1
0
-0.1
-0.2
-0.3
-0.4
-0.5
50
0
-50
-150
-100
-50
0
50
100
150

Figure 9.

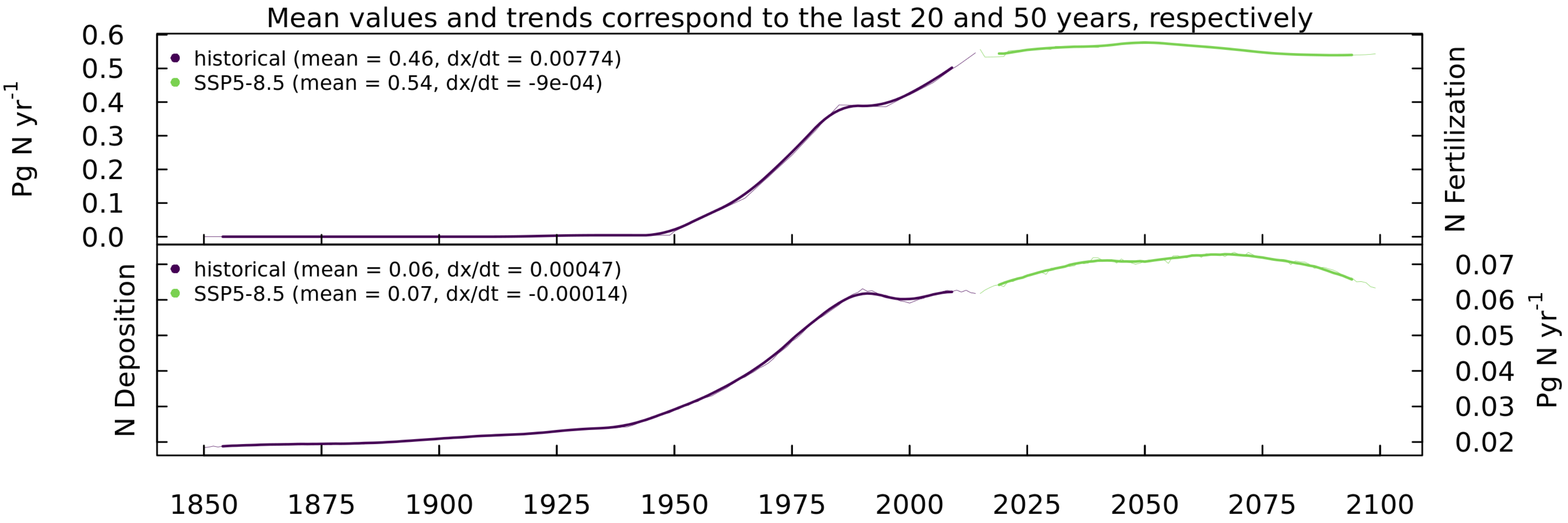

Mean values and trends correspond to the last 20 and 50 years, respectively
historical (mean = 0.46, dx/dt = 0.00774)
SSP5-8.5 (mean = 0.54, dx/dt = -9e-04)
historical (mean = 0.06, dx/dt = 0.00047)
SSP5-8.5 (mean = 0.07, dx/dt = -0.00014)
Pg N yr-1
N Fertilization
N Deposition
Pg N yr-1
0.0
0.1
0.2
0.3
0.4
0.5
0.6
0.02
0.03
0.04
0.05
0.06
0.07
1850
1875
1900
1925
1950
1975
2000
2025
2050
2075
2100